BMC Biology

RESEARCH ARTICLE

Open Access

The first embryonic landscape of G-quadruplexes related to myogenesis

Lijin Guo[1,2], Weiling Huang[1,3], Qi Wen[1], Siyu Zhang[1], Farhad Bordbar[1], Zhengzhong Xiao[2] and Qinghua Nie[1*]

Abstract

Background DNA G-quadruplexes (G4s) represent a distinctive class of non-canonical DNA secondary structures. Despite their recognition as potential therapeutic targets in some cancers, the developmental role of G4 structures remains enigmatic. Mammalian embryonic myogenesis studies are hindered by limitations, prompting the use of chicken embryo-derived myoblasts as a model to explore G4 dynamics. This study aims to reveal the embryonic G4s landscape and elucidate the underlying mechanisms for candidate G4s that influence embryonic myogenesis.

Results This investigation unveils a significant reduction in G4s abundance during myogenesis. G4s stabilizer pyridostatin impedes embryonic myogenesis, emphasizing the regulatory role of G4s in this process. G4 Cut&Tag sequencing and RNA-seq analyses identify potential G4s and DEGs influencing embryonic myogenesis. Integration of G4 and DEG candidates identifies 32 G4s located in promoter regions capable of modulating gene transcription. WGBS elucidates DNA methylation dynamics during embryonic myogenesis. Coordinating transcriptome data with DNA G4s and DNA methylation profiles constructs a G4-DMR-DEG network, revealing nine interaction pairs. Notably, the *NFATC2* promoter region sequence is confirmed to form a G4 structure, reducing promoter mCpG content and upregulating *NFATC2* transcriptional activity.

Conclusions This comprehensive study unravels the first embryonic genomic G4s landscape, highlighting the regulatory role of *NFATC2* G4 in orchestrating transcriptional activity through promoter DNA methylation during myogenesis.

Keywords G4s landscape, Embryonic period, Myogenesis, DNA methylation

Background

DNA G-quadruplexes (G4s) are unique DNA secondary structures formed from two or more stacked G-tetrads, which are square coplanar arrays of four guanine bases [1]. DNA G4 structures were first found in telomere regions [2]. As a kind of non-classical DNA structures, G4s have been confirmed with various roles in numerous biological processes, including transcription, DNA replication, telomere protection, and so on [3–7]. The G4s in the promoter regions are thought to be involved in the regulation of transcription [8]. Several DNA G4s have been discovered in the promoter region of oncogenes, suggesting a strategy to inhibit tumorigenesis by inducing G4s to block transcription of these oncogenes [3, 9, 10]. Multiple small molecule ligands that intercalate

*Correspondence:
Qinghua Nie
nqinghua@scau.edu.cn
[1] State Key Laboratory of Livestock and Poultry Breeding, & Lingnan Guangdong Laboratory of Agriculture, & Guangdong Provincial Key Lab of Agro-Animal Genomics and Molecular Breeding & Key Lab of Chicken Genetics, Breeding and Reproduction, Ministry of Agriculture and Rural Affair, South China Agricultural University, Guangzhou 510642, China
[2] Henry Fok School of Biology and Agriculture, Shaoguan University, Shaoguan 512005, China
[3] School of Biological and Behavioural Sciences, Queen Mary University of London, London, UK

into the G4 structure have been developed to target tumor-related G4s. It has been confirmed that TMPyP4 suppresses *c-MYC*, while pyridostatin (PDS) shows an inhibition of telomere dysfunction and cancer growth [11–13]. Based on the regulation of transcriptional activity mediated by the G4s promoter region of oncogenesis genes, more selective G4 ligands have been developed for use in cancer therapy, such as CX-3543, CX-5461, and PDC12 [14–16]. Although the role of G4 in oncogenesis is well known, it is still unclear how endogenous G4s realize their role in normal biological processes. G4 structures have been reported to be widely distributed in the genomes of various organisms [17]. There is increasing evidence that G4 structures are present in the promoter of many genes [18–20], suggesting that G4s could be considered as a kind of structural motif to regulate the transcriptional activity of genes.

Our understanding and knowledge of the cell lineages and muscle morphogenesis of skeletal muscle development is largely based on the avian model [21], which is tremendously conducive to the study of muscle development during the embryonic period. Birds are advantageous for embryonic development research because they lay eggs, making embryos easy to obtain and handle without harming pregnant mammals, with controlled and short incubation times. Embryonic myogenesis is controlled by myogenic regulatory factors (MRFs), including myogenic differentiation 1 (MyoD1), myogenin (MyoG), myogenic factor 5 (Myf5), and myogenic regulatory factor 4 (MRF4) [22]. Myf5, MyoD1, and MRF4 have been reported to play roles in myogenic determination, which directs progenitor cells to form the muscle lineage during development, while the downstream effector myogenin, together with MyoD1 and MRF4, activates the myogenic differentiation program [23, 24]. The fusion of myoblast into myotubes is one of the most important steps of myogenesis, which requires precise spatial and temporal regulation during embryonic development and is coordinately controlled by multiple regulatory factors [25].

Notably, G-quadruplex (G4) density is associated with stem cell pluripotency, and G4 structures are lost during lineage specification as human stem cells differentiate [26]. Furthermore, increased G4 density is highly detrimental to myoblast differentiation by inhibiting *MyoD1* transcription under TMPyP4 exposure in the C2C12 cell line [27]. Additionally, abnormal expression of *DUX4*, which leads to facioscapulohumeral muscular dystrophy (FSHD), can be alleviated by targeting G4 structures in the *DUX4* gene [28]. These findings suggest that G4-mediated transcriptional regulation plays a crucial role in both muscle development and muscle disease. In contemporary research, G4 structures have been identified not only in DNA but also in RNA molecules. The helicase *DHX36* is essential for muscle regeneration as it promotes satellite cell (SC) proliferation by unwinding RNA G-quadruplex (rG4) structures in the 5′ untranslated regions of target mRNAs, particularly influencing the translation of Gnai2 mRNA [29]. Methodologically, the development of rG4-targeting L-RNA aptamers is expanding the current rG4 toolkit, enabling innovative rG4-related applications, such as rG4-SELEX [30]. Although G4s have been referred with genes transcriptional activity, the myogenesis-related genes regulated by G4s in birds at the embryonic stage are not yet well understood.

The landscape of G4s at the whole genome level in different species has been reported under some prediction models [17, 31–33]. G4s are relatively conserved in evolutionary conservation analyses, while the number, length, and density of G4s generally increase during evolution in different species [32, 33]. It was reported that birds have the highest proportion of genes with G4 motifs in the promoter compared to other 14 species [33]. In addition, the G4 motifs were more enriched in transcriptional regulatory regions [17, 34]. However, to date, there is no report on how G4 regulates gene transcription in bird embryo.

In addition to G4, there are many other regulatory factors in the gene promoter region, such as CpG methylation, that share a common feature, namely that both are generally localized in regions of high GC content [35]. Although a few studies have reported the interaction between G4s and DNA methylation [33, 36], the understanding of this interaction remains largely unclear. In this study, we aim to comprehensively uncover the dynamics of the G4s landscape, mCpG, and gene transcription during myoblast myogenesis.

Results

G4 may participate in embryonic myogenesis

During embryonic muscle development, myogenesis is a highly complex and essential process that is regulated by a convoluted network of intrinsic and extrinsic factors. To understand G4s potential in embryonic development, we investigated whether the abundance of G4s changes during chicken myoblast differentiation. Myoblast was stimulated to differentiate in DMEM medium with 4% HS until they developed into multinucleated myotubes. During myoblast differentiation, G4s abundance was gradually downregulated (Fig. 1A), suggesting that myoblast global DNA G4 might be modulated in myotube fusion under the stress of low nutrient/energy supply. This phenomenon was also observed in mouse myoblast differentiation (Additional File 1: Fig. S1A). Based on this evidence, we hypothesized that DNA G4 may be a regulator during embryonic myogenesis.

Here, PDS, which is generally regarded as a trigger or stabilizer for global DNA G4s, was used to induce the formation/stabilization of G4 in myoblasts (Fig. 1B). It was shown that G4s density increases with a dose-dependent manner. After treating with PDS, the cell cycle of myoblasts was measured by cell cycle analysis (Fig. 1C). As G4s increased, the proportion of cells that transitioned from G1 phase to S phase was greatly reduced ($P<0.0001$). Furthermore, an EdU assay was performed to quantify G4-mediated cell proliferation. Similar to the results of cell cycle analysis, the EdU assay also revealed an agonist of PDS on regulating cell proliferation (Fig. 1D). In addition, PDS treatment was able to increase *CCNB2* (Cyclin B2) and *CCND1* (Cyclin D1) mRNA levels, while downregulating *CDKN1B* (cyclin-dependent kinase inhibitor 1B) mRNA expression (Fig. 1E). Our data illustrated that PDS could impede myoblast proliferation. Here, the *CDKN1B* mRNA did not decrease in a dose-independent manner, which may be caused by possible DNA damage mediated by high-dose PDS [12, 37]. On the other hand, myoblast differentiation-related genes, including *MyoD1*, *MyoG*, and *MyHC* (myosin heavy chain), were downregulated in a dose-independent manner (Fig. 1E). In addition, Desmin protein level also decreased after PDS treatment (Additional file 1: Fig. S1B). In addition, MyoG positive cell proportion significantly decreased under PDS treatment in a dose-independent manner (Fig. 1F). To understand the specific role of PDS on myoblast differentiation, myoblasts treated with 10 μM, 20 μM, and 30 μM PDS were induced to differentiate. Interestingly, the index of myotube fusion gradually decreased with increasing PDS concentration (Fig. 1G). These results revealed that PDS altered G4 homeostasis which inhibits embryonic myogenic differentiation.

Global genome G4 dynamic during myogenic differentiation

G4s has been identified as a potential modulator of embryonic myogenic differentiation, but the global distribution of G4s in the chicken genome is still unknown. Moreover, the dynamics of G4s at the embryonic stage also remains to be characterized. Cut & Tag, a technique for exploring protein-DNA interactions, has been extended to map G4s in global genome DNA [38, 39]. Here, Cut & Tag assay and genome sequencing were performed in GM and DM (DM3) to investigate the G4 structures in the global genome by using BG4 antibody. The size of fragments obtained from Cut & Tag was analyzed and it was found that DM had a higher frequency in the size of 400 to 800 bp, while GM had a higher frequency in the size of 150 to 200 bp (Additional file 1: Fig. S2A). The generated data were filtered and mapped. The mapping rate was 88.82% and 88.30% for the NC and PDS groups, respectively (Additional file 2: Table S1). The reads mapped in the genome were mainly located at ± 2 Kb region of TSS/TES, and the distribution of reads was very similar between DM and GM as it is close to TSS (Additional file 1: Fig. S2B).

Peak calling was then performed and 7812 peaks in GM and 5511 peaks in DM were detected. Their percentage of the genome in DM is much higher in DM than in GM (Additional file 2: Table S1). Here, MAnorm tool was used to adjust the difference between the groups and the

(See figure on next page.)

Fig. 1 G4s participate in myoblast differentiation. **A** Chicken primary myoblasts treated with GM, DM for 24 h (DM1), 48 h (DM2), 72 h (DM3), and 96 h (DM4) were collected and performed G4-immunofluorescence staining ($n=3$). The G4-stained cells proportion was quantified in a flow cytometry. Fluorescence value ≥ 10^4 was considered as the threshold for G4-stained cells. Ordinary one-way ANOVA was used to analyze the difference among groups. Different letters represent $P<0.05$. **B** The left panel is the chemical structure formula of PDS. Different PDS concentrations (10 μM, 20 μM, and 30 μM) were set up in treating myoblasts for 48 h and DMSO was considered as the negative control. After treating with PDS, the cells were collected and used to perform a G4-immunofluorescence staining ($n=6$). The G4-stained cells proportion was quantified in a flow cytometry. Fluorescence value ≥ 10^3 was considered as the threshold for G4-stained cells. Student's *t*-test was used to analyze the difference among groups. ****$P<0.0001$. **C** Myoblasts treated with PDS for 48 h were collected and used to perform a cell cycle analysis by PI staining ($n=6$). Stained cells were measured in a clow cytometry and cell cycle was analyzed by using FlowJo. Student's *t*-test was used to analyze the difference among groups. *$P<0.05$, **$P<0.01$, ****$P<0.0001$. **D** Myoblasts treated with PDS for 48 h were collected and used to perform a EdU analysis ($n=3$). Stained cells were captured in a fluorescence microscope. The scale length was 100 μm. EdU-stained cell rate was quantified in flow cytometry and fluorescence value ≥ 10^4 was considered as the threshold for EdU-stained cells. Student's *t*-test was used to analyze the difference among groups. *$P<0.05$, **$P<0.01$, ****$P<0.0001$. **E** Myoblasts treated with PDS for 48 h were collected and total RNA was extracted. The mRNA levels of *CCNB2*, *CCND1*, *CDKN1B*, *MyoD1*, *MyoG*, and *MyHC* were quantified by qPCR in Applied Biosystems QuantStudio 5. Student's *t*-test was used to analyze the difference among groups. *$P<0.05$, **$P<0.01$, ***$P<0.001$, ****$P<0.0001$. **F** Different PDS concentrations (10 μM, 20 μM, and 30 μM) were set up in treating myoblasts for 48 h. The cells were collected and used to perform a MyoG-immunofluorescence staining ($n=6$). The G4-stained cells proportion was quantified in a flow cytometry. Fluorescence value ≥ 10^4 was considered as the threshold for MyoG-stained cells. Student's *t*-test was used to analyze the difference among groups. ****$P<0.0001$. **G** Different PDS concentrations (10 μM, 20 μM, and 30 μM) were set up in inducing myotube fusion for 72 h ($n=3$). Myotubes were labelled by MyHC immunofluorescence and captured in a fluorescence microscope. ImageJ was used to measure myotube fusion index. Student's *t*-test was used to analyze the difference among groups. **$P<0.01$, ***$P<0.001$, ****$P<0.0001$

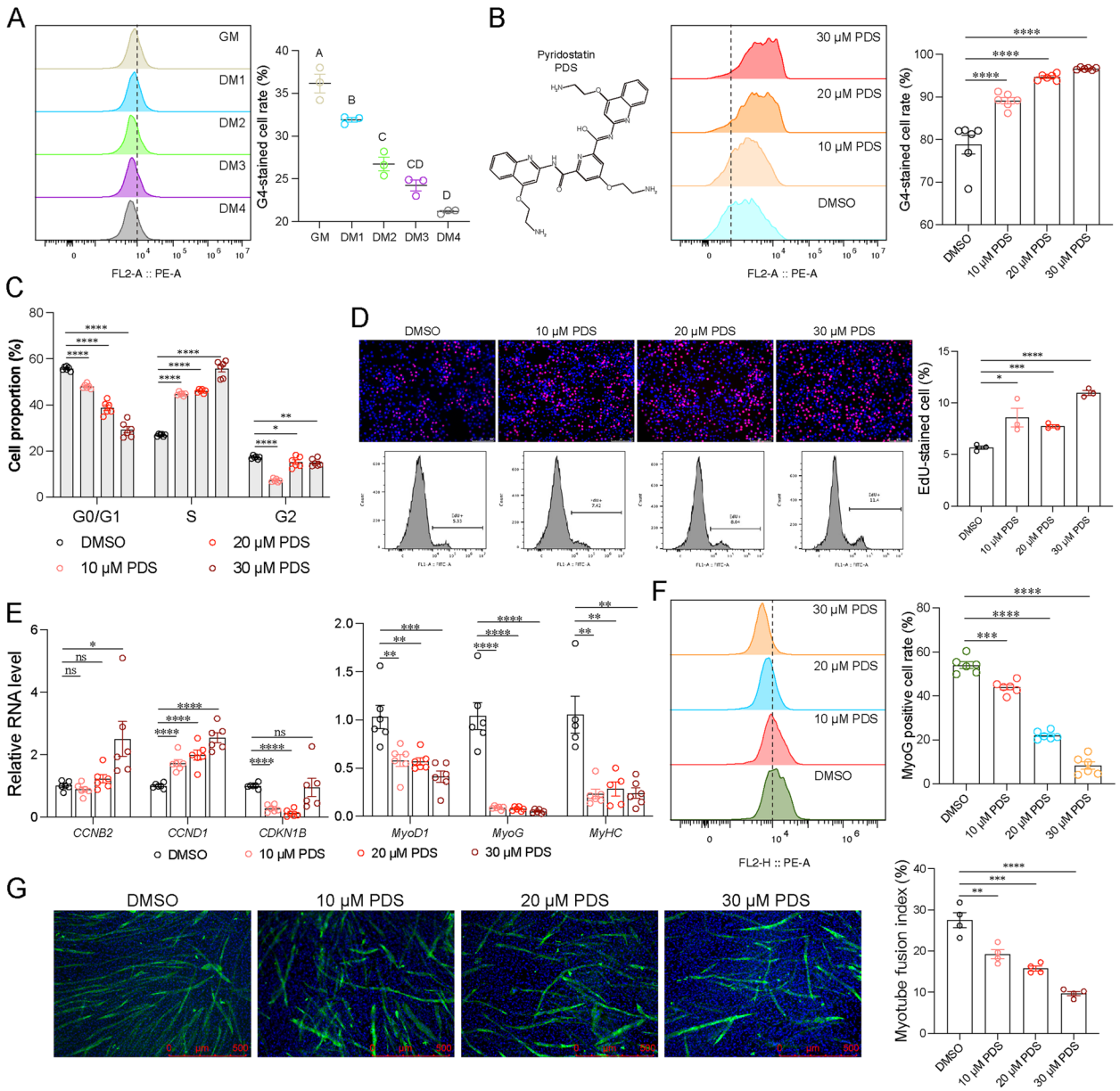

Fig. 1 (See legend on previous page.)

P-value < 0.05 and |M-value| > 1 were set as the criteria for differential peaks (DPs). A total of 615 DPs were generated and of which 395 DPs upregulated while 220 DPs downregulated (Fig. 2A and Additional file 2: Table S2). G4 DPs are not present on several MRF genes (Additional file 2: Table S2). However, one G4 peak was found in the promoter region of *MyoD1*, although it was not different between GM and DM (Additional file 1: Fig. S3), which is possible that in vitro differentiation condition was not sufficient to perturb it.

The DPs were primarily located in the region of the promoter (≤ 1 kb) (67.64%) (Fig. 2B), revealing a potential regulation of transcription. Analysis of the depth distribution of DPs reads in the upstream and downstream sections showed a very similar trend in the peak distribution between DM and GM, but the abundance in DM was significantly higher than in GM (Fig. 2C). GO enrichment analysis was performed to comprehensively assess the biological function of these DPs. For GM, the DPs could be enriched in *cardiomyocyte differentiation*, *positive regulation of MAP kinase activity*, *positive regulation of cardiomyocyte differentiation*, and *MAP-kinase scaffold activity*. For DM, the DPs were enriched in the *positive regulation of mesenchymal cell proliferation* and the

regulation of the *MAPK cascade* (Fig. 2D). Based on the distribution characteristics of DPs, which are mainly distributed in the promoter region, we defined these DPs as promoter-derived differential peaks (PDPs) and analyzed their biological functions separately. The results of GO enrichment show that they can be associated with *mesenchyme migration*, *substrate-dependent cell migration*, *chondrocyte development*, and *regulation of* the *MAPK cascade* (Fig. 2E). Moreover, KEGG pathway enrichment analysis revealed that these PDPs may be enriched in some basic biological regulatory pathways such as *TGF – beta signaling*, *FoxO signaling*, *MAPK signaling*, and *pyruvate metabolism* (Fig. 2F). The results indicate a potential regulatory role of G4 in modulating these signaling pathways to further alter myoblast differentiation.

Transcriptome dynamics during embryonic myogenic differentiation

Based on the above data, the potential role of G4s on embryonic myogenic differentiation was confirmed. However, the specific transcriptome dynamics of myoblasts during myogenic differentiation is still unclear. High-through RNA-seq has been an indispensable tool for transcriptome-wide analysis of differential gene expression [40]. To unfold the dynamics of the myoblast transcriptome before and after differentiation induction, RNA-seq was performed. The raw data generated from RNA-seq was submitted to SRA database. An overview of the RNA-seq data can be found in Additional file 2: Table S3. The clean reads generated from this sequencing were mapped to the GRCg7b genome. The criteria for screening differentially expressed genes (DEGs) were P-value < 0.05 and |log2FC| > 1. A total of 808 DEGs were screened, of which 454 DEGs were downregulated while 354 DEGs were upregulated (Additional file 2: Table S4 and Fig. 3A). The top 30 DEGs were selected to show their expression between groups (Fig. 3B). Among them, *A4GALT* (A4GALT – alpha 1,4-galactosyltransferase), the most significant DEG, was upregulated in DM. Moreover, myosin heavy chain 1 beta-subtype (*MYH1B*) was also upregulated in DM. To fully understand the biological function of these DEGs, they were used in GO enrichment analysis (Additional file 2: Table S5 and Fig. 3C). For the biological processes, these DEGs could be enriched in several GO terms of multiple skeletal muscle development, including *muscle contraction*, p*ositive regulation of stress fiber assembly,* a*ttachment of mitotic spindle microtubules to kinetochore*, and s*keletal muscle thin filament assembly*. For cellular component, these DEGs could be enriched in *myofibril*, *myosin filament*, and *Z disc*, which are essential components in the fusion of myotubes. The enriched molecular functions are also significantly associated with muscle development, such as *calmodulin binding*, *muscle alpha-actinin binding*, *actin filament biding*, *microtubule motor activity*, and *structural constituent of muscle*. Interestingly, DM treatment resulted in upregulation of the entire *MYH1* family, including *MYH1A*, *MYH1B*, *MYH1C*, *MYH1D*, *MYH1E*, *MYH1F*, and *MYH1G*, suggesting a strong promotion of the *myosin filament* biological process, which may be primarily responsible for the acceleration of embryonic myogenic differentiation in DM.

Candidate G4s associated with embryonic myoblast differentiation

RNA-seq analysis and G4 Cut & Tag sequencing analysis revealed the potential regulatory factors modulating myogenesis. To further clarify the transcriptome dynamics mediated by G4, 454 upregulated DEGs, 354 downregulated DEGs, 395 hyper DPs, and 220 hypo DPs were comparatively analyzed (Fig. 4A). There were 16, 7, 22, and 0 genes in the overlay of upregulated DEGs-hyper DPs, downregulated DEGs-hyper DPs, downregulated DEGs-hypo DPs, and upregulated DEGs-hypo DPs, respectively (Additional file 2: Table S6). In addition, the correlation analysis results showed that DPs

(See figure on next page.)

Fig. 2 Cut & Tag sequencing of G4 for myoblast DM-vs-GM. **A** The M-A plot for DPs generated from GM and DM. Every DP is shown as a dot, and the color of the dots represents -$\log_{10}$P-value. Horizontal axis represents normalized A value and vertical axis represents normalized M value. Peaks are colored based on the significance of the differences (p-value). Higher MA values with lower p-values suggest a higher likelihood that the peak is a differential peak. **B** The distribution of identified differential peaks (DPs) across genomic functional elements was annotated using ChIPseeker. The annotation results were statistically analyzed and represented as a pie chart, of which different colored regions indicate peaks annotated to various genomic functional elements. **C** The deeptools software was used to analyze the uniquely compared sequences of DM and GM and analyze their distribution in the differentially bound peaks and the upstream and downstream 2-kb regions. Horizontal axis showing the differentially bound peaks and the 2-kb regions before and after DM and GM, while the vertical axis showing the average value of the reads abundance in the region. **D** The chord plots of top 10 GO terms in GO enrichment analysis for GM DPs and DM DPs. The left-half circle represents the DPs enriched in the top 10 GO terms, of which light red represents upregulated DPs in DM and light blue represents upregulated DPs in GM. The right-half circle represents the top 10 GO terms. **E** The top 10 GO terms DPs enriched for biological process, cellular component, and molecular function. The vertical axis is the GO term name and the horizontal axis is -$\log_{10}$$P$-value. **F** The top 20 KEGG pathways DPs enriched. Horizontal axis represents enrichment score. Entries with larger bubbles contain more target genes and bubble color varies from blue-white-yellow–red. The smaller the enrichment p-value, the greater the significance

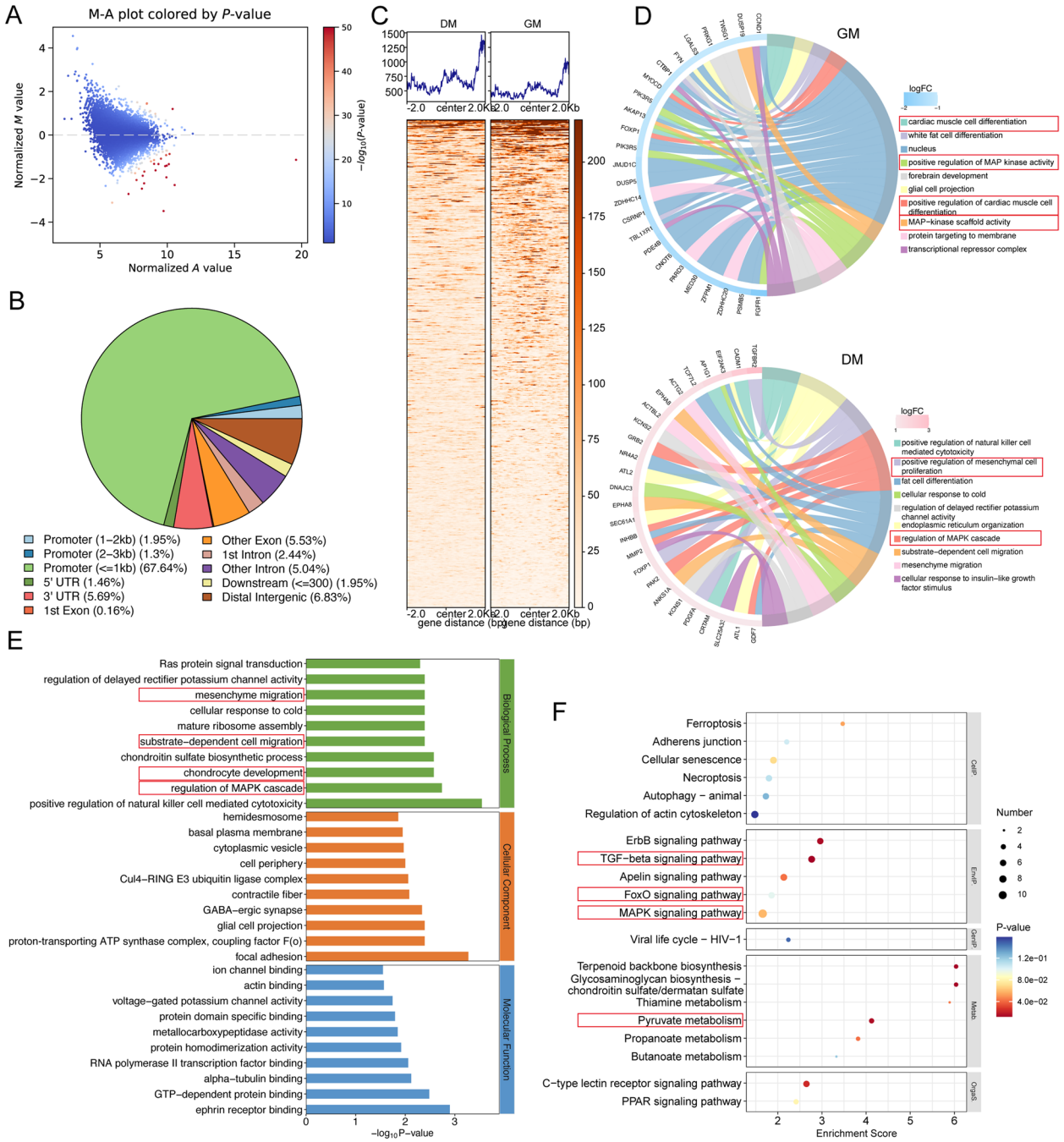

Fig. 2 (See legend on previous page.)

were positively correlated with DEGs ($R=0.61$ and $P=1.1e^{-5}$) (Fig. 4B). Most of these DPs were located in the promoter region (Fig. 4C), suggesting a potential role for these DPs in transcriptional regulation. PPI analysis, GO enrichment, and KEGG pathway enrichment analysis of these DEGs were combined (Fig. 4D). The most significant GO term was the process of *cholesterol biosynthesis* (*HMGCS1*, *IDI2*, and *INSIG1*). In addition, *cell proliferation* (*DLGAP5*, *ERBB4*, and *ID4*) and *myofibrils* (*MYH1G* and *TMOD1*) were also enriched. The most significant KEGG pathway was the *biosynthesis* of the *Terpenoid backbone* (*HMGCS1* and *IDI2*). *TGF-beta signaling pathway* (*ID4* and *TGFBR2*) and *MAPK signaling pathway* (*ERBB4*, *PLA2G4A*, and *TGFBR2*) were also enriched. The abundance of these genes in G4 Cut & Tag-seq and associated RNA-seq is shown in Fig. 4E,

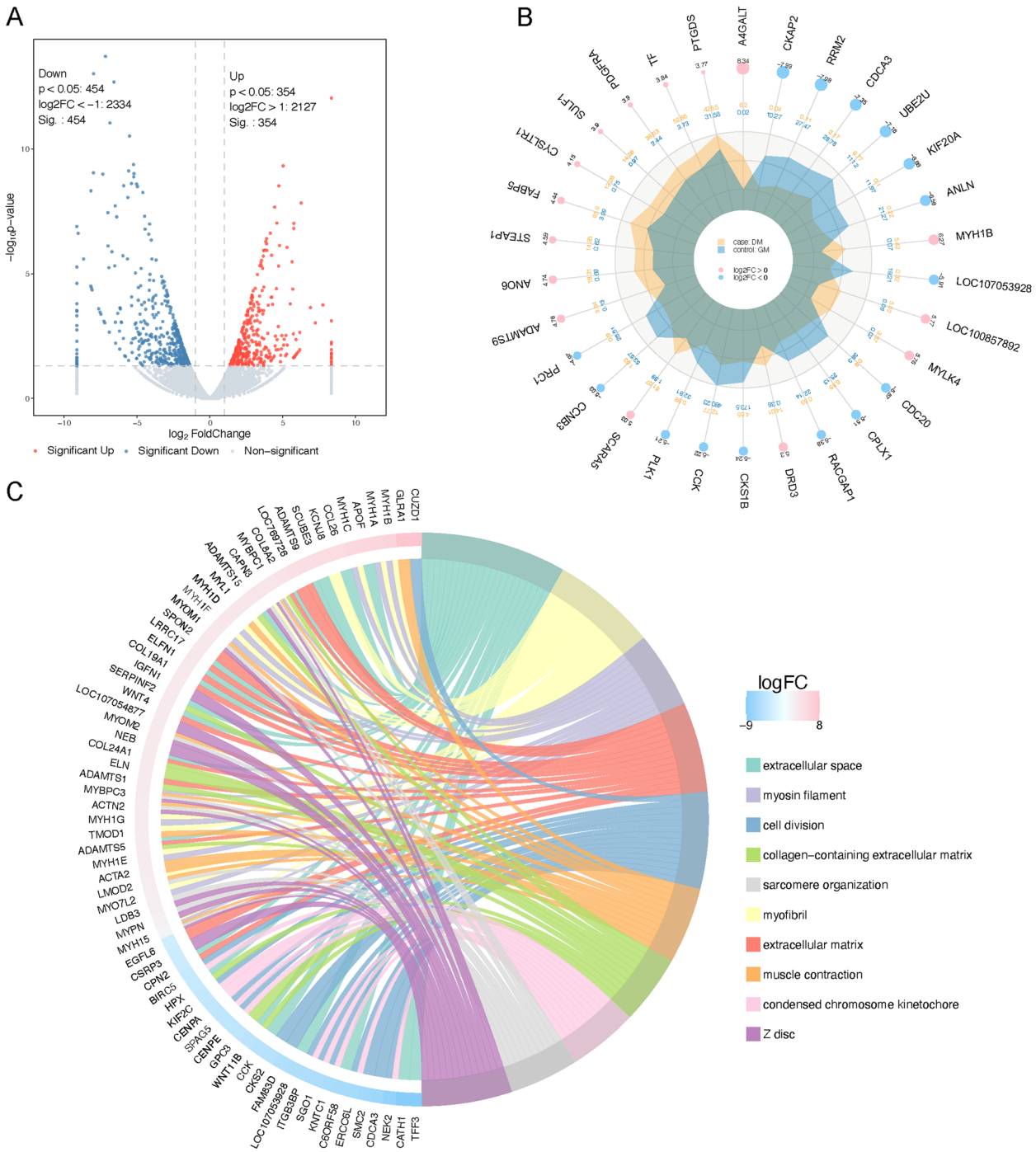

Fig. 3 RNA-seq analysis for myoblast DM-vs-GM. **A** DESeq software was used to normalize the count number of each sample gene, calculate the multiplicity of differences, and test the significance of differences using NB (negative binomial distribution test). Screened DEGs generated from GM and DM were reflected into a volcano plot, of which the light-blue features represent the downregulated DEGs, while the light-red features represent the upregulated DEGs. The horizontal axis represents log_2FC and the vertical axis represents -log_{10}*P*-value. **B** The top 30 DEGs with the smallest *p*-value were displayed in a radar plot. For the first circle, the light red circle represents upregulated DEGs while light blue represents downregulated DEGs. The circle size depends on log_2(FC) value. For the second circle, the light-yellow value represents the DEG average expression in PDS group while the light-blue value represents the DEG average expression in GM group. For the third circle, the peak represents DEG gene expression in different groups. **C** The chord plot of top 10 GO terms in GO enrichment analysis. The left-half circle represents the DEGs enriched in the top 10 GO terms, of which light red represents upregulated DEGs and light blue represents downregulated DEGs. The right-half circle represents the top 10 GO terms

as well as their fold change, in which *HMGCS1*, *IDI2*, *INSIG1*, *DLGAP5*, and *ID4* were downregulated, while the other five genes were upregulated. Among them, DPs in *IDI2* and *DLGAP5* are negatively correlated with RNA expression, while others are positively correlated. Myofibrillar protein is the terminal product of myogenic differentiation and the most basic component of myofibers. *MYH1G* and *TMOD1*, which are enriched in *Myofibril* GO term, were both enriched in G4 Cut & Tag and differentially expressed between GM and DM, suggesting that they may be regulated by G4 and thus affect the myogenic differentiation. Here, the differential G4 peak sequences of *TMOD1* and *MYH1G* were used to predict potential G4 PQSs. Two PQSs and one PQS were respectively identified (Table 1). Cut & Tag PCR was performed and it was found that these PQSs were all differentially expressed between GM and DM (Fig. 4F). Additionally, their RNA levels were also quantified by qPCR (Fig. 4G). Taken together, our data identified several potential G4 candidates that may affect gene transcription, which could be responsible for embryonic myogenic differentiation.

DNA methylation in embryonic myogenesis

DNA methylation is a major epigenetic modification that can influence gene transcription. Although DNA methylation is widely recognized as an important epigenetic regulator during myogenic differentiation, DNA methylation and gene expression patterns in chicken myoblast differentiation have been poorly understood. Whole genome bisulfite sequencing (WGBS) is considered the "gold standard" of DNA methylation research, which combines with bisulfite processing and high-throughput sequencing techniques, to achieve the methylation analysis of single C-base in the whole genome, which is suitable for the construction of the whole genome fine methylation map [41]. Here, the same batch samples were used in a WGBS (Additional file 1: Fig. S4A). The summary of methylation is shown in Additional file 2: Table S7. The DNA methylation level in DM (36.61%) was higher compared to GM (34.11%). Of the three types of methylation, mCG (mCpG) accounted for the majority, in both DM and GM (Additional file 1: Fig. S4B). The methyl level at gene elements profiling showed a lower level for CHG and CHH in DM (Additional file 1: Fig. S4C), with no differences at promoter, exon, intron, and downstream. For CpG, the methyl level in DM was higher at promoter, exon, and downstream, while it was lower at intron (Fig. 5A). In general, DNA methylation levels are significantly increased in promoters and downstream regions during myogenic differentiation.

To further clarify the specific methylation dynamics during myogenic differentiation, a DMR analysis was performed. A window of 1000 bp was simply set as a window and DMR regions with significant differences were analyzed according to the degree and significance of differences in window methylation levels (differences $\geq 10\%$ and P-value ≤ 0.05). Based on the above result, the CpG methylation contributed the most to global DNA methylation. Here, we analyzed mCpG separately and 517,491 DMRs were fully captured based on these screening criteria. After annotation of these DMRs, they were used in GO and KEGG pathway enrichment analysis (Additional file 1: Fig. S5). These DMRs could be enriched in the *activation of protein kinase activity*, *Wnt signaling pathway*, and *stress-activated protein kinase signaling cascade* (Additional file 1: Fig. S5A), which could be responsible for myogenic differentiation. In KEGG enrichment analysis, these DMRs were enriched in *MAPK signaling pathway*, m*TOR signaling pathway, phosphatidylinositol signaling system*, and *Wnt signaling pathway* (Additional file 1: Fig. S5B). It has been confirmed that promoter regions show the greatest methylation differences during myogenic differentiation (Fig. 5A), which is also the most important element for transcriptional regulation. A total of 20,579 DMRs were detected, of which 1897 DMRs were hyper-methylated and 3085 DMRs were hypomethylated (Fig. 5B). These DMRs could be enriched with Go terms of the *meiotic cell cycle* and *cellular response to starvation* (Fig. 5C), suggesting that methylation of the promoter regions may indeed respond directly to the initiation of embryonic myogenic differentiation.

(See figure on next page.)

Fig. 4 Potential candidates regulated by G4 during myogenic differentiation. **A** The Veen plot for the cross-talk between DEGs and DPs. The light-blue, light-red, light-yellow, and light-green circles represent down-regulated DEGs, up-regulated DEGs, hyper DPs and hypo DPs, respectively. **B** The correlation of the cross-talk between log2FC of DEGs and log2FC of DPs was calculated by using Pearson's correlation coefficient analysis. The vertical axis represents log2FC for DEGs, while the horizontal axis represents log2FC for G4 DPs. **C** The gene element distribution of DPs, which were associated with gene expression change. **D** The PPI analysis, GO term enrichment analysis and KEGG pathway enrichment analysis for 45 DEGs were combinate in Cytoscape. *p*-value was shown by gradual color. **E** The abundance and their fold change of the 10 DEGs and DPs between GM and DM. **F** The G4 Cut & Tag of products were used to perform a PCR to validate the DPs regions in *TMOD1* and *MYH1G*, which have been predicted with G4 PQSs ($n = 3$). Student's *t*-test was used to analyze the difference among groups. ** $P < 0.01$. **G** The total RNA was extracted from DM and GM, then the mRNA levels of *MYH1G* and *TMOD1* were quantified by qPCR ($n = 6$). Student's *t*-test was used to analyze the difference among groups and ****$P < 0.0001$

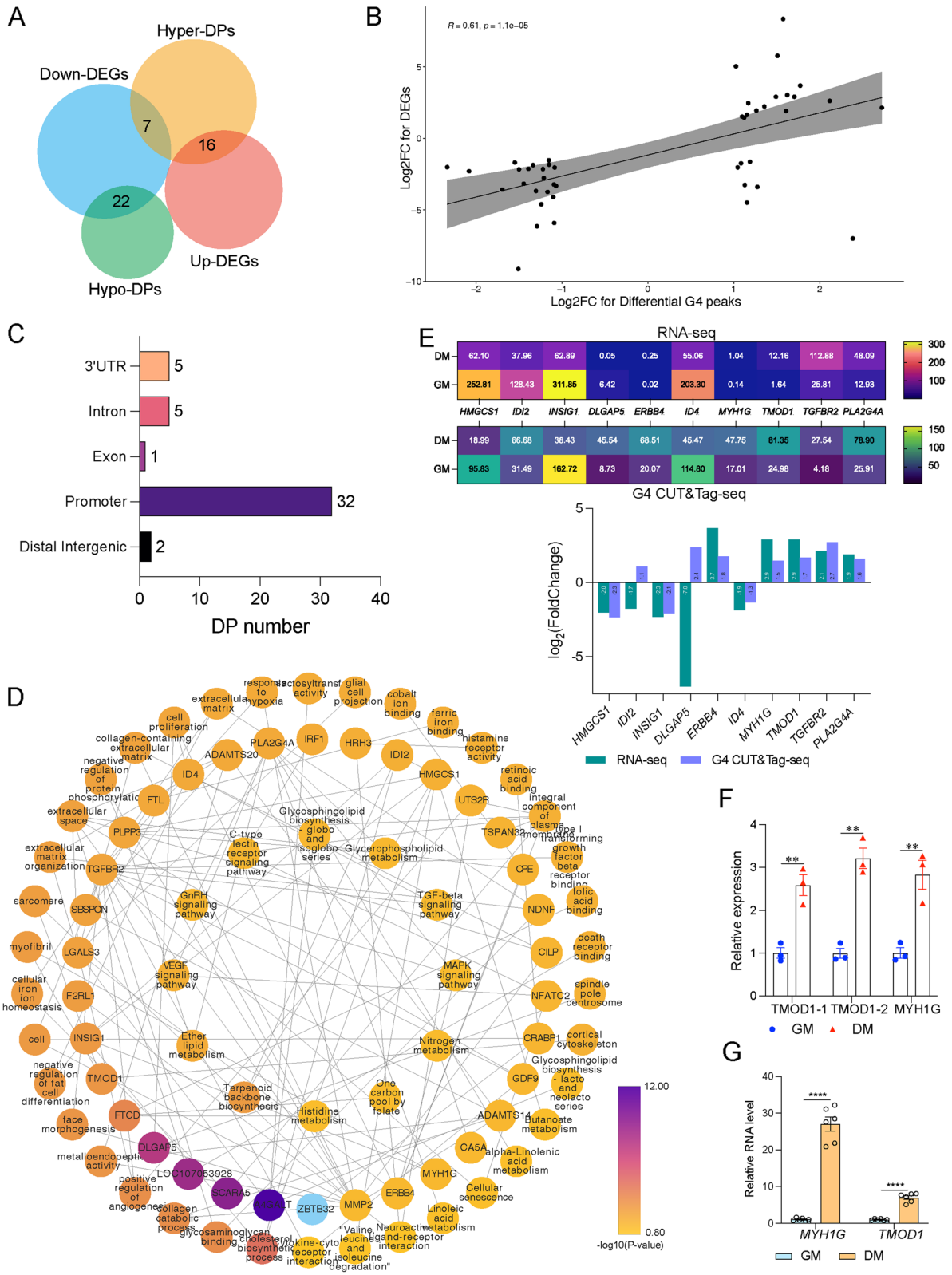

Fig. 4 (See legend on previous page.)

Table 1 The information of PQSs in *MYH1G* and *TMOD1*

Name	Distance to TSS	PQS	G-score
TMOD1-1	435 nt	**GGGGGG**CCTGGCTTAAA**GGG**A**GGG**	51
TMOD1-2	571 nt	**GGG**TGGTCGT**GGG**TGGCCAGGTGTGT**GGG**A**GGG**	50
MYH1G	5615 nt	**GGG**TTGAGCTGTGTCA**GGG**GA**GGG**TCAGGTT**GGG**	51

Gene promoter region sequences were submitted to QGRS (accession link: https://bioinformatics.ramapo.edu/QGRS/analyze.php) for PQS prediction, with the parameter of max length ≤ 40 and min G-group ≥ 3 and loop size ≤ 20. The G-score represents the potential that PQS forms a G4 structure. Bold letters represent the G-group sequences. Here, the promoter regions sequences of *TMOD1* and *MYH1G* were submitted for PQS prediction

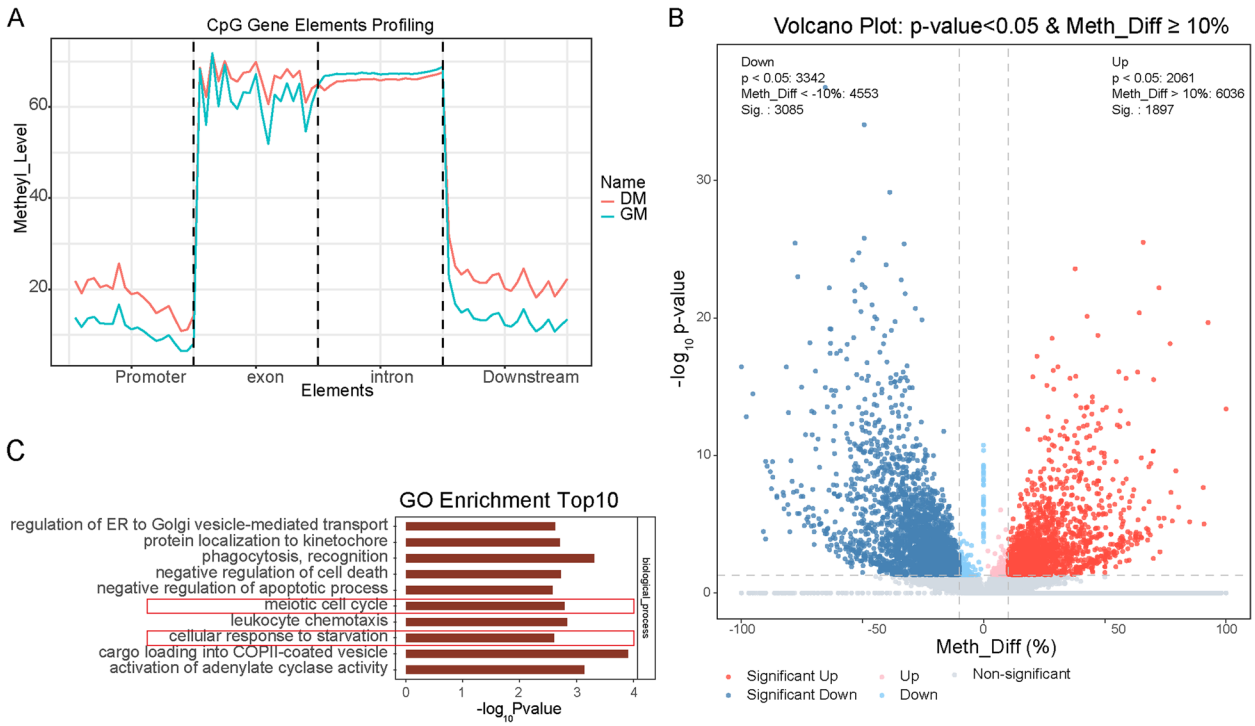

Fig. 5 The DNA methylation dynamics during myogenic differentiation. **A** Gene elements profiling analysis by CpG-type methylation was visualized in a line plot. The element segments including genebody, upstream 2 kb (promoter) and downstream 2 kb, were divided into 20 bin, and the methylation level in each bin reflected the general trend of methylation level change of gene segment. The average methylation level for all genes in each bin was reflected in to the line plot. The light blue line represents GM, while the pink line represents DM. **B** CG-type DMRs located at promoter region (DMPs) were visualized in a volcano plot. FC ≥ 10% and $P < 0.05$ were considered as the threshold for DMPs. The blue plots represent the DMPs $P < 0.05$ and FC ≤ −10%, red plots represent the DMPs $P < 0.05$ and FC ≥ 10%. **C** The top 10 Biological Process GO terms enriched by CG-type DMPs. The vertical axis is the GO term name and the horizontal axis is $-\log_{10}P$-value

DNA methylation regulates gene transcription during embryonic myogenesis

To comprehensively observe which genes were regulated by DNA methylation during myogenic differentiation, omics data generated from RNA-seq and WGBS were integrated. The selected CpG-type DMRs located in promoter regions were used for association analysis with DEGs. A total of 196 DMR-DEG pairs were identified, of which 26 were hypermethylated DMR-upregulated DEGs (Hyper-up), 48 were Hypo-up, 42 were Hyper-down, and 80 were Hypo-down (Fig. 6A). These 196 DEGs were analyzed in GO enrichment analysis, and they were significantly enriched at the *protein localization to kinetochore*, *cell division*, and *mitotic chromosome condensation* (Fig. 6B), which are associated with cell proliferation.

Interestingly, these DEGs associated with cell proliferation were all downregulated, including *NCAPG*, *NUSAP1*, *NCAPD3*, *CDCA3*, *MASTL*, *SGO1*, *ERCC6L*, *KIF11*, *SPC25*, *CCNB1*, *PTTG2*, *SMC2*, *MTBP*, *TTK*, and *MIS12*. The promoter regions of *NCAPG*, *NCAPD3*, *MASTL*, and *MTBP* were hypermethylated, while others

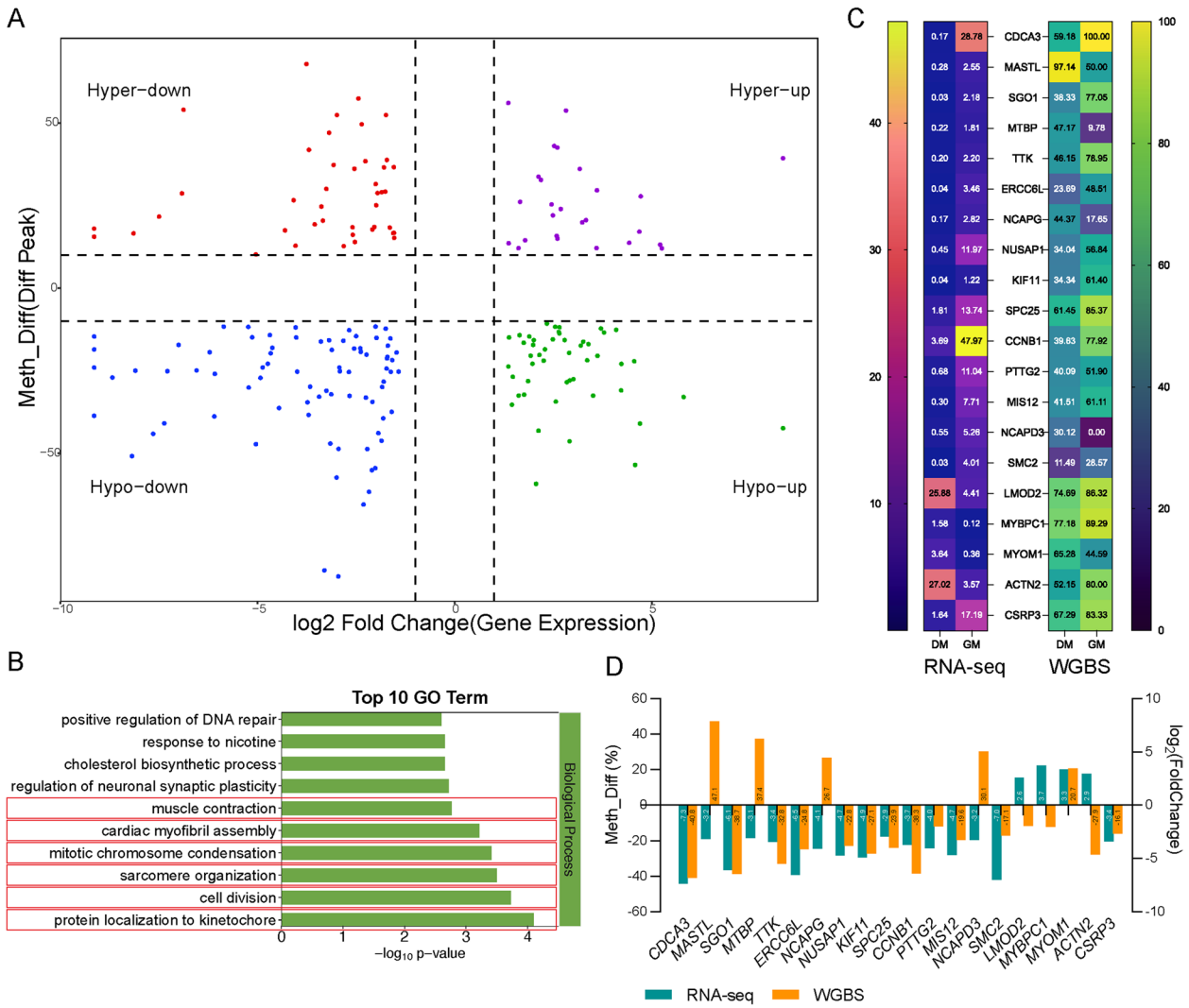

Fig. 6 Promoter methylation regulates myogenic differentiation. **A** The cross-talk between DEGs and DMRs. The DMRs were CpG-type methylated and were located at promoter regions. The horizontal axis represents gene expression, shown by Log_2Fold Change, while vertical axis represents differential peaks, shown by percentage. **B** The top 10 GO term in biological process, enriched by 196 DEGs. **C** The mRNA levels and promoter region CpG-type methyl levels of genes related to cell proliferation and myogenic differentiation in RNA-seq and WGBS, respectively. **D** The fold change for DEGs abundance and the methyl difference percentage change for DMRs in RNA-seq and WGBS, respectively

were hypomethylated (Fig. 6C, D). Moreover, they were also able to enrich in several biological processes related to myogenic differentiation, such as *muscle contraction*, *cardiac myofibril assembly*, and *sarcomere organization* (Fig. 6B). The enriched DEGs, including *LMOD2*, *MYBPC1*, and *ACTN2*, were all upregulated, accompanied by hypomethylation of promoter regions (Fig. 6C, D). Taken together, the dynamic changes in promoter methylation of genes related to cell proliferation and myogenic differentiation affect gene transcription and further drive the process of embryonic myogenic differentiation.

G4-DMR-DEG network construction in embryonic myogenesis

G4s and methylation are both essential epigenetic factors that may influence myogenesis, but their coordination is still unclear. The above results have confirmed that both G4s and promoter region methylation can regulate gene transcription during myogenic differentiation. There are 45 intersections between DPs and DEGs (Fig. 4B) and 196 intersections between DMRs and DEGs (Fig. 6B). A G4-DMR-DEG network was constructed by integrating the two intersections and nine overlays between two intersections were obtained (Fig. 7A). They were listed in Fig. 7B, including *RPESP*, *HRH3*, *IDI2*, *LOC112532533*,

MBP, *MYOCD*, *NFATC2*, *PLA2G4A*, and *TGFBR2*. With the exception of the G4 DP at *IDI2*, other G4 DPs were positively correlated with the fold change of their transcripts. In addition, the mRNA levels of *IDI2*, *LOC112532533*, and *MBP* were positively correlated with the methyl levels of their promoter regions, contradicting the principle that methylation in the promoter region inhibits gene transcription. Subsequently, the sequences of the other six peaks which were pulled down by G4 Cut & Tag, were used to predict PQS (predicted quadruplex sequence) that had the potential to form G4 structure in QGRS Mapper. Herein, the PQSs were identified within 3000 bp before TSS were captured and only three DEGs were predicted to have PQS of more than 30 G-score consistent with this criterion (Table 2, Fig. 7C and Additional file 1: Fig. S6). qPCR was used to verify the mRNA

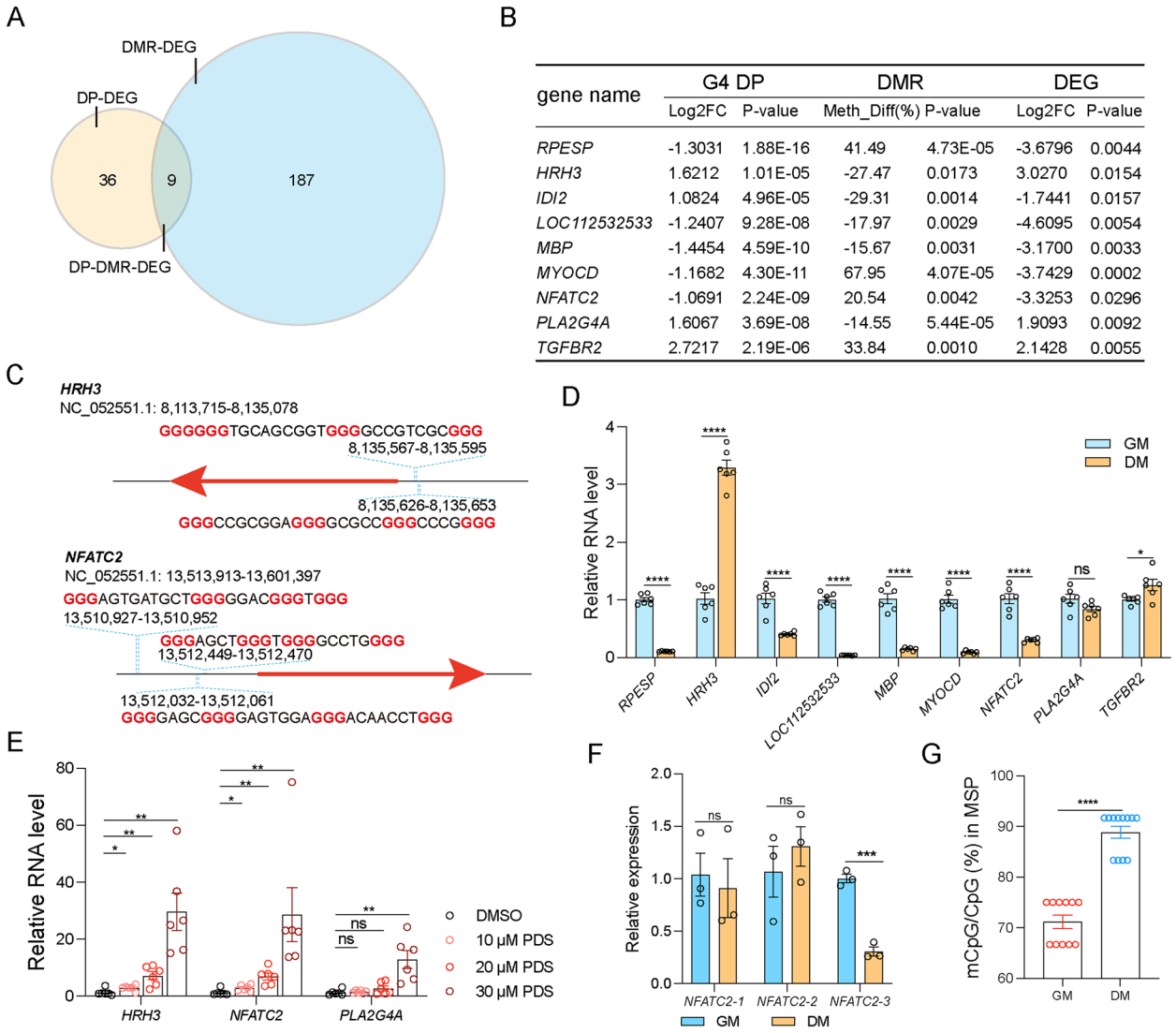

gene name	G4 DP		DMR		DEG	
	Log2FC	P-value	Meth_Diff(%)	P-value	Log2FC	P-value
RPESP	-1.3031	1.88E-16	41.49	4.73E-05	-3.6796	0.0044
HRH3	1.6212	1.01E-05	-27.47	0.0173	3.0270	0.0154
IDI2	1.0824	4.96E-05	-29.31	0.0014	-1.7441	0.0157
LOC112532533	-1.2407	9.28E-08	-17.97	0.0029	-4.6095	0.0054
MBP	-1.4454	4.59E-10	-15.67	0.0031	-3.1700	0.0033
MYOCD	-1.1682	4.30E-11	67.95	4.07E-05	-3.7429	0.0002
NFATC2	-1.0691	2.24E-09	20.54	0.0042	-3.3253	0.0296
PLA2G4A	1.6067	3.69E-08	-14.55	5.44E-05	1.9093	0.0092
TGFBR2	2.7217	2.19E-06	33.84	0.0010	2.1428	0.0055

Fig. 7 G4-DMR-DEG network reveals a G4 candidate for myogenesis. **A** The Venn plot for the overlay indicated the intersection between G4DP-DEG and DMR-DEG. The light-yellow circle represents 45 G4DP-DEG interactions, while the light-blue circle represents 196 DMR-DEG interactions. **B** The 9 candidates derived from the 9 G4DP-DMR-DEG interactions information during myogenesis, including FC and *P*-value. **C** The 9 candidates were used to predict the PQSs in their promoter regions, of which *HRH3* and *NFATC3* respectively exhibited 2 and 3 high G-score PQSs. **D** Total RNA was extracted from GM and DM and used to quantify the mRNA levels of 9 DEGs by qPCR ($n=6$). Student's *t*-test was used to analyze the difference among groups. * $P<0.05$ and **** $P<0.0001$. **E** Total RNA was extracted from myoblast treated with PDS and used to quantify the mRNA levels of *HRH3*, *NFATC2*, and *PLA2G4A* by qPCR ($n=6$). Student's *t*-test was used to analyze the difference among groups. * $P<0.05$ and ** $P<0.01$. **F** G4 Cut & Tag was performed in GM and DM and the products were used to run a PCR to validate the PQS *NFATC2* G4s difference between GM and DM ($n=3$). Student's *t*-test was used to analyze the difference among groups and *** $P<0.001$. **G** The mCpG/CpG (%) of promoter region in GM ($n=11$) and DM ($n=12$) was quantified by MSP. Student's *t*-test was used to analyze the difference among groups and *** $P<0.001$

levels of the DEGs between DM and GM. It was found that the expression trends of these DEGs in qPCR were consistent with RNA-seq, except for *PLA2G4A*, and *TGFBR2* (Fig. 7D). To further verify whether the mRNA dynamics of *HRH3*, *NFATC2*, and *PLA2G4A* were mediated by potential G4s in the promoter regions during myogenic differentiation, their mRNA levels were quantified upon treatment with PDS (Fig. 7E). Interestingly, all of their mRNA levels could be upregulated by PDS and have a dose-dependent effect. PDS has been shown to inhibit myogenesis (Fig. 1F). Herein, *NFATC2* was downregulated during myogenic differentiation which is diametric to PDS treatment, suggesting that it may be the primary factor inhibiting myogenic differentiation mediated by G4s. Taken together, *NFATC2* was considered a primary candidate. Cut & Tag PCR was performed to validate the three PQSs and *NFATC2-3* was found to be significantly enriched in GM (Fig. 7F), which was consistent with G4 Cut & Tag sequencing. Furthermore, *NFATC2-3* sequence was considered as a potential G4. In addition, the methyl level at the CpG of the *NFATC2* promoter in GM and DM was quantified by MSP (methylation-specific PCR). The methylated CpG (mCpG) on *NFATC2* promoter in DM was higher compared to GM (Fig. 7G), which was consistent WGBS result.

G4 promotes NFATC2 transcription by inhibiting NFATC2 promoter methylation

The PQSs of *NFATC2* were considered as candidate G4s, which were responsible for myogenesis. However, validation for their G4 structure is still required. Herein, we performed a PSA to verify whether they can form a G4 structure. Consistent with our speculation, linear sequence could be amplified in PCR, while the G4 structure could not (Fig. 8A), confirming that *NFATC2-2* PQS can form a G4 structure. In conjunction with the Cut & Tag PCR result, *NFATC2* was hypothesized as a potential epigenetic factor responsible for the regulation of myogenesis. To verify whether ch*NFATC2* G4 could regulate the *NFATC2* transcription process, the specific ASO that could disrupt G4 formation was synthesized. The principle of ASO treatment assay is shown in Fig. 8B. G4 formation was completely disrupted after

Table 2 The information of PQSs in candidates

Name	Distance to TSS	PQS	G-score
HRH3-1	489 nt	**GGGGGG**TGCAGCGGTG**GGG**CCGTCGC**GGG**	33
HRH3-2	548 nt	**GGG**CCGCGGA**GGG**GCGCC**GGG**CCCG**GGG**	39
NFATC2-1	2961 nt	**GGG**AGTGATGCT**GGG**GGAC**GGG**T**GGG**	34
NFATC2-2	1443 nt	**GGG**AGCT**GGG**TG**GGG**CCTG**GGG**	40
NFATC2-3	1852 nt	**GGG**GAGC**GGG**AGGTGAG**GGG**ACAACCT**GGG**	39
PLA2G4A	59 nt	**GGGGGG**AGGC**GGG**TGACTCACGGC**GGG**	31

Gene promoter region sequences were submitted to QGRS (accession link: https://bioinformatics.ramapo.edu/QGRS/analyze.php) for PQS prediction, with the parameter of max length ≤ 40 and min G-group ≥ 3 and loop size ≤ 20. The G-score represents the potential that PQS forms a G4 structure. Bold letters represent the G-group sequences. Here, the promoter region sequences of *HRH3*, *NFATC2*, and *PLA3G4A* were submitted for PQS prediction

(See figure on next page.)

Fig. 8 G4 promotes *NFATC2* transcription by changing promoter mCpG. **A** The left panel is a schematic diagram of PSA. Simply put, after G4 is formed, it is not easy or cannot be unlocked to initiate the PCR reaction. The G4 and mutant G4 sequences were amplified with a specific FAM labelled primer, under the G4 induction or not. PCR product couldn't be obtained with a G4 induction, while PCR product could be obtained without G4 induction. The PSA on mutant G4 sequence was used as a negative control ($n = 3$). **B** The upper panel is the principle schematic diagram that *NFATC2* G4 specific ASO regulates G4 formation. During G4 induction, ASO and unspecific single-strand DNA were separately added. The specific primer was used to PCR amplification. Double-strand DNA (PCR product) could be obtained with ASO treatment, while double-strand DNA could not be obtained with ASO control ($n = 3$). **C** Total RNA was extracted from myoblasts that treated with *NFATC2* G4 specific ASO or 5-AZA and mRNA level of *NFATC2* was quantified by qPCR ($n = 6$). Student's t-test was used to analyze the difference among groups and $^{*}P < 0.05$. **D** DNA was extracted from myoblasts that treated with *NFATC2* G4 specific ASO or 5-AZA and mCpG level was quantified by MSP ($n = 6$ for NC, $n = 11$ for ASO control, $n = 12$ for ASO and $n = 12$ for ASO + 5-AZA). Student's *t*-test was used to analyze the difference among groups. $^{*}P < 0.05$ and $^{****}P < 0.0001$. **E** Total RNA was extracted from the myoblasts treated with *NFATC2* overexpression or knockdown and mRNA levels of *MyoD1*, *MyoG* and *MyHC* were quantified by qPCR ($n = 6$). Student's *t*-test was used to analyze the difference among groups. $^{*}P < 0.05$ and $^{**}P < 0.01$. **F** Myoblasts treated with *NFATC2* overexpression or knockdown for 48 h were collect for MyoG-immunofluorescence staining and quantified in a flow cytometry. The fluorescence value ≥ 10^4 was considered as the threshold for MyoG-stained cells. Student's *t*-test was used to analyze the difference among groups. $^{**}P < 0.01$, $^{****}P < 0.0001$. **G** Myoblasts treated with *NFATC2* overexpression and knockdown in inducing myotube fusion for 72 h ($n = 3$). Myotubes were labelled by MyHC immunofluorescence and captured in a fluorescence microscope. ImageJ was used to measure myotube fusion index. Student's *t*-test was used to analyze the difference among groups. $^{**}P < 0.01$, $^{****}P < 0.0001$

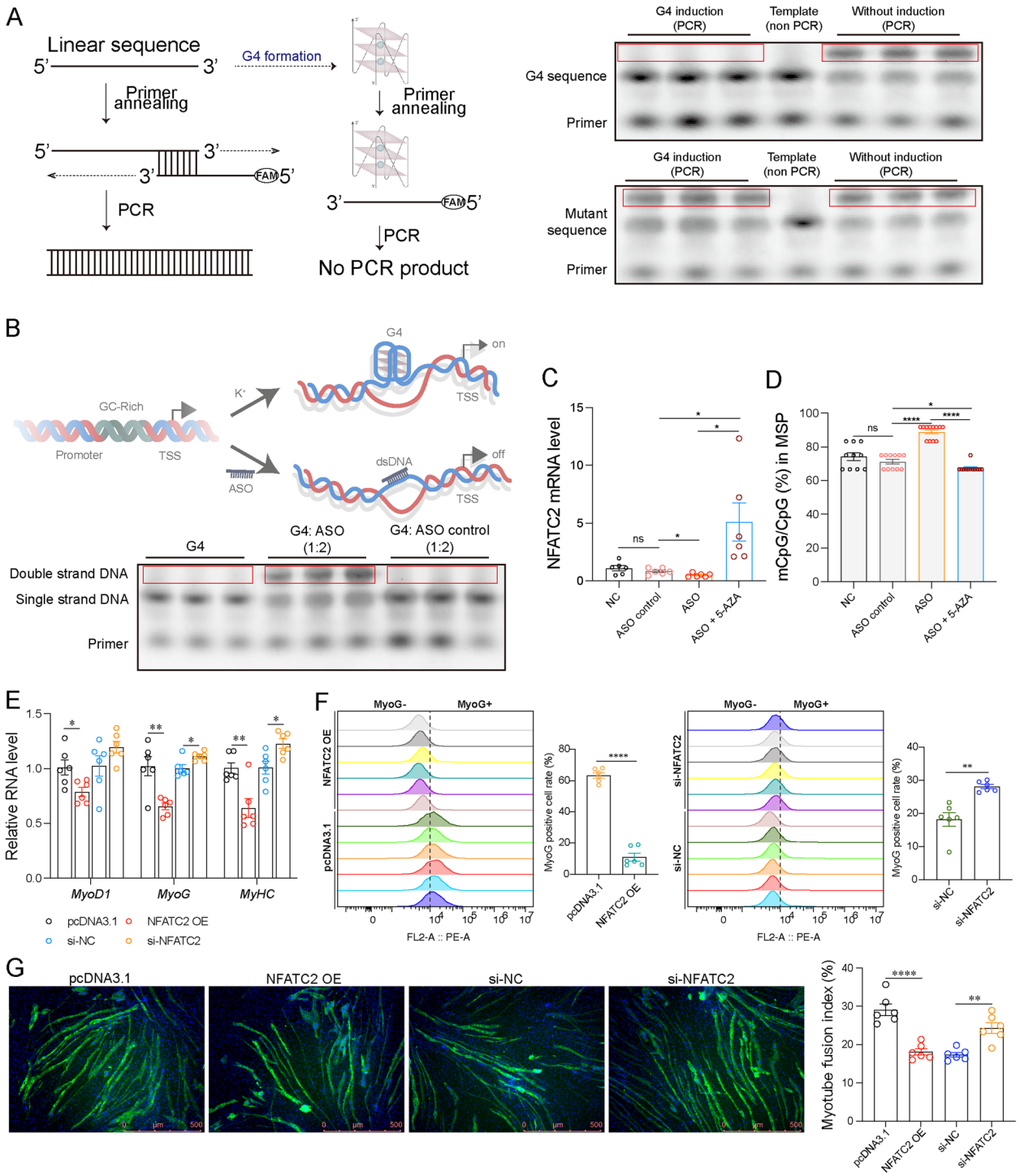

Fig. 8 (See legend on previous page.)

treating with ASO oligonucleotides, whereas G4 could be formed after treating with unspecific ASO oligonucleotides (Fig. 8B). Furthermore, the specific ASO was used to treat myoblasts and the mRNA level of *NFATC2* was quantified. It was found that ASO could downregulate *NFATC2* mRNA level (Fig. 8C). This result suggests that G4 formation on *NFATC2* promoter region could inhibit *NFATC2* transcription. Additionally, MSP was performed after treating with ASO. mCpG level of *NFATC2* promoter region was significantly increased (Fig. 8D),

demonstrating an inhibitory effect of G4 on DNA methylation of the *NFATC2* promoter. To validate whether G4-mediated mCpG dynamics at the *NFATC2* promoter could alter transcriptional activity, 5-AZA, a common inhibitor of DNA methylation, was added. Interestingly, 5-AZA was able to reverse the ASO-mediated increase in mCpG, which was accompanied by a strong upregulation of *NFATC2* mRNA levels (Fig. 8C, D). Taken together, *NFATC2* G4 was able to inhibit mCpG which could upregulate transcriptional activity.

Considering *NFATC2* transcription activity downregulation mediated by reducing G4 during myoblast differentiation, its potential in myoblast differentiation needs to be further validated. Here, *NFATC2* overexpression plasmid was constructed and specific siRNA (si-NFATC2) was designed and synthesized to overexpress and knockdown *NFATC2* in myoblast. After overexpressing *NFATC2* in myoblast, the mRNA levels of *MyoD1*, *MyoG*, and *MyHC* were all downregulated, while the knockdown of *NFATC2* would increase these mRNA level (Fig. 8E). Furthermore, *NFATC2* decreased MyoG positive rate and its downregulation was able to increase MyoG positive cell (Fig. 8F). Moreover, *NFATC2* low expression could promote myotube fusion (Fig. 8G). Overall, *NFATC2* expression downregulation boosts myoblast differentiation.

Discussion

DNA G4 is a class of non-classical DNA secondary structures related to the transcriptional activity of genes [1, 19, 20]. Although the chicken G4 promoter region of chickens is particularly abundant in the predictions, there have been no studies directly reporting the function and mechanism of G4 in chickens [33]. In this study, we report that G4 is directly associated with embryonic myogenic differentiation and downregulation of G4 abundance in the *NFATC2* promoter region can increase mCpG levels in order to decrease mRNA levels of *NFATC2*.

Myoblast differentiation at the embryonic stage is a convoluted process that mainly involves the fusion of myoblasts and the secondary fusion of myoblasts to form myotubes [42]. Intra-envelope cation balance mediated by potassium–calcium channels during embryonic development plays crucial role for myogenic differentiation. The concentration of potassium and calcium ions in MuSCs is to some extent negatively correlated with the capacity for myogenesis [26, 43–45]. Among them, the monovalent cations are required for stacking of G-quartets, typically potassium in a cellular context [46]. Our data show that the abundance of G4s gradually decreases during myogenesis (Fig. 1A). This phenomenon could be due to the dynamics of monovalent cations suggesting that G4s may be involved in myogenesis to some extent. G4-ligand pyridostatin (PDS) has been widely used as a stabilizer for DNA G4, which could increase the overall level of G4s [47]. At this point, PDS treatment was able to promote myoblast proliferation and inhibits myoblast differentiation (Fig. 1), revealing a negative effect of whole G4s level on myogenesis. However, the distribution of G4s in the chicken is still unknown.

To comprehensively uncover the G4 landscape in the chicken genome, a G4 Cut & Tag was performed in myoblasts with GM treatment or DM treatment and a total of 615 DPs were obtained (Fig. 2A). Although the number of G4 structures per nucleus in chicken cells is lower compared to human cells, the proportion of G4s in the promoter region of chicken cells is higher in comparison with human [33]. It was reported that the average frequency of potential G4 motifs in the whole genome was only 0.107, while the frequency in the region from − 1000 bp to TSS increased to 0.768 [48], revealing the transcriptional regulatory potential of G4s. Based on the G4 Cut & Tag data, most DPs (67.64%) were localized in the promoter region (− 1000 bp to TSS), which is consistent with other studies.

To further assess the regulation of transcriptional activity mediated by these G4s, RNA-seq was performed. By combining the G4 Cut & Tag sequencing and RNA-seq, a total of 45 DP-DEG pairs were identified (Fig. 4A), of which 32 DPs were localized in the promoter regions. Among them, MYH1G and TMOD1 were both highly expressed in DM (Fig. 4F). MYH1G is a type of myosin heavy chains that has been implicated as a terminal product for myoblast differentiation [49, 50]. In contrast to MYH1, tropomodulins (TMODs) are capping proteins that specify the length of thin filament to optimize skeletal muscle function during myofibril formation [51, 52], not to mention that TMOD1 was required for skeletal muscle stem cell differentiation [53]. The enrichment of DPs in G4 Cut & Tag of *MYH1G* and *TMOD1* along with their RNA levels suggest that G4s can directly promote myoblast terminal differentiation by increasing these myofibril genes.

DNA methylation plays a crucial role as epigenetic factors on numerous biological processes. It has been reported that G4s can influence the transcriptional activities of genes by regulating adjacent DNA methylation [54, 55]. G4s were positively correlated with CpG density, while there was an inverse correlation with mCpG/CpG [54, 56]. Here, we performed a WGBS to clarify their potential interaction during myogenesis. The promoter region methyl level of DM was higher compared to GM, which was in contrast to G4s (Fig. 1A and Fig. 5A). Based on G4 prediction and validation, *NFATC2* was considered as a candidate due to

its promoter could form a G4 that inhibits the mCpG portion of the promoter. *NFATC2* G4 and mRNA levels were downregulated, while mCpG level was increased. The NFATC2-IL4 axis was widely considered to be an activator for secondary fusion of myoblasts to myotubes and *NFATC2* was required for myotube fusion by maintaining MHC production [57, 58]. NFATC2 was able to play the role of a transcription factor for *IL4* secreted by the myotube to target the IL4R on the surface of myoblast, which drives secondary fusion [59]. Secondary fusion from myoblast to myotube mediated by the NFATC2-IL4 axis was dependent on IL4R [42]. In this study, *NFATC2* was downregulated in DM, which was in contrast to other reports. This could be due to the chicken IL4R having too little homology with mammals. The role of *NFATC2* in myogenesis may require completely different mechanisms in mammals which needs further validation. Overall, the abundance of G4s is reduced during myogenic differentiation, in contrast to promoter methylation. Among them, the downregulation of G4 of the *NFATC2* promoter leads to increased DNA methylation, which in turn reduces the mRNA level of *NFATC2*.

Conclusions

As a class of non-classical DNA secondary structure, G4s have been referred with capabilities on regulating genes transcriptional activity, but its dynamics and how does it mediate transcriptome dynamics in the embryonic stage are not yet well understood. Birds are tremendously conducive to the study of muscle development during the embryonic period. In this study, embryo chicks were used as the model for exploring embryonic G4s dynamics during myogenesis. Considering G4s abundance reduction during myogenesis and the myogenic differentiation inhibition mediated by G4s inducer, G4s were inferred to be associated with embryonic myogenesis. Embryonic G4s were comprehensively revealed during myogenic differentiation and totally 6777 G4 peaks were obtained, of which 45 DPs associated with the transcription of embryonic myogenesis-related DEGs were identified. Based on the cooperation on myogenesis mediated by DNA methylation, 196 DMR-DEG pairs were identified. By constructing a G4-DMR-DEG network, nine DP-DMR-DEG pairs were further identified, of which the promoter of *NFATC2* was capable of forming a G4 structure to inhibit promoter mCpG to promote *NFATC2* transcription.

Methods

Animal experiments and ethic statement

All animal experiments in this research were approved by the Animal Welfare Committee of South China Agricultural University (Approved ID: SCAU#2021F074). All animal experiments were conducted in compliance with the regulations of the People's Republic of China for the control of experimental animals. The fertilized eggs derived from Mahuang Chicken, were purchased from Xufeng Husbandry Co., Ltd. (Kaiping, China).

Cell culture, cell transfection, and cell differentiation

The chicken myoblast was isolated as described in our previous study [60]. Myoblast was cultured in growth medium (GM), consisting of DMEM medium (GBICO, CA, US) with 20% fetal bovine serum (GBICO, CA, US) and 1% penicillin/streptomycin (Invitrogen, CA, US) in a 37 °C cell incubator with 5% CO_2.

For cell transfection, Lipofectamine 3000 Reagent Kit (Invitrogen, CA, US) was used by following its instruction when the cells were 80% confluent. The DNA transfection dose was 1 μg per well in a 12-well plate and 2.5 μg per well in a 6-well plate.

For cell differentiation, differentiation induction medium (DM) consisting of DMEM medium (GBICO, CA, US) supplemented with 4% horse serum (GBICO, CA, US) and 1% penicillin/streptomycin (Invitrogen, CA, US) was used for myoblast differentiation for 72 h when myoblast reached 100% confluence.

For PDS treatment, 10 μM, 20 μM, and 30 μM PDS (MCE, NJ, US) were added to the growth or differentiation medium to culture the myoblasts when the cell confluence was higher than 90%, while equal DMSO was used as a negative control.

For anti-sense oligonucleotide (ASO) treatment, 0.5 mM ASO was used to transfect the myoblasts and the cells were collected for DNA or RNA extraction after 48 h of transfection. A random oligonucleotide of the same length was used as a negative control. The ASO information is listed in Additional file 2: Table S8; 5 μM 5-azacytidine (5-AZA) (Solarbio, Beijing, China) was used to inhibit DNA methyltransferase in myoblasts.

5-Ethynyl-2′-deoxyuridine (EdU) assay

Cell-Light EdU Apollo488 in vitro Kit and Cell-Light EdU Apollo567 in vitro Kit (RioBio, Guangdong, China) were used to observe the cell proliferation ratio according to the manufacturer's protocol. For Apollo567 dye staining with EdU and Hoechst, myoblasts were captured in visual fields using a DMi8 microscope (Leica, Wetzlar, Germany). For staining with Apollo488 dye EdU, myoblasts were flushed in a flow cytometry (Beckman, US) and the data were analyzed using FlowJo 10.0 software.

Quantitative PCR (qPCR)

Total RNA of cells was isolated using Trizol reagent (Magen, Guangzhou, China) according to the manufacturer's instruction. The first strand of cDNA synthesis was performed using HiScriptR II Q RT SuperMix for qPCR (+gDNA wiper) (Vazyme, Nanjing, China) according to its protocol. Finally, qPCR was performed using ChamQ Universal SYBR qPCR Master Mix (Vazyme, Nanjing, China) in an ABI QuantStudio 5 instrument (Thermo Fisher, NY, US) according to the protocol. GAPDH was used as a reference gene in qPCR. The primers used in qPCR were designed in NCBI Primer-Blast and synthesized by Tsingke company (Guangzhou, China). The primer sequence information is listed in Additional file 2: Table S8.

MSP (methylation-specific PCR)

MSP was performed to quantified mCpG in this study. EpiArt DNA Methylation Bisulfite Kit (Vazyme, Nanjing, China) was used to transfect cytosine (C) into thymine (T) in DNA bisulfite library as its manufacturer. 2×EpiArt HS Taq Master Mix (Dye Plus) (Vazyme, Nanjing, China) was used to run the PCR reaction according to its standard construction. MSP primers were designed in MethPrimer (accession link: http://www.urogene.org/cgi-bin/methprimer/methprimer.cgi). The primers were listed in Additional file 2: Table S8. PCR products were cloned into pUC57 plasmid and transfected into DH5a cell. The sanger sequence for monoclonal colonies was used to quantify mCpG levels.

Western blot

Gene expression at the protein level was analyzed by western blot. Total protein was isolated using ice-cold radio immunoprecipitation (RIPA) lysis buffer (Tsingke, Guangzhou, China) with 1% phenylmethyl sulfonyl fluoride (PMSF) (Biosharp, Shanghai, China) in ice for 20 min. After centrifugation at 4 °C, 13,000×*g* for 15 min, the supernatant was transfected into a new tube. Then the sample was incubated with 5×SDS protein loading buffer (Servier, Guangzhou, China) at 95 °C for 10 min. The protein was isolated in 4–20% SDS-PAGE at 120 V for 90 min. Subsequently, the protein was transfected into a PVDF membrane (BioRad, US) at 200 mA for 2 h. After blocking with 5% BSA (Servier, Guangzhou, China), the PVDF membrane was incubated overnight at 4 °C with the primary antibody. Anti-Desmin (1:1000, DSHB) was used in this study. The anti-mouse secondary antibody (1:10,000, proteintech) was incubated for 1 h at room temperature. BeyoECL Plus Kit (Beyotime, Shanghai, China) was used in chemiluminescence reaction. No-Stain™ Protein Labeling Reagent (Invitrogen, CA, US) was used for total protein normalization, according to its instruction, which was used as the load reference. The original images were shown in Additional file 3.

Cleavage under target and tagmentation (Cut & Tag) and library construction

Cut & Tag was performed using the Hyperactive Universal Cut & Tag Assay Kit for Illumina (Vazyme, Nanjing, China). This protocol was slightly modified. Myoblasts treated with differentiation medium (DM) and growth medium (GM) were used in Cut & Tag. They were counted in an automated cell counter (Countstar, Shanghai, China). About 10^5 cells were harvested with Trypsin-0.25% EDTA (GBICO, CA, US) and cell nuclei were extracted with NE buffer. They were then incubated with activated ConA Beads. Subsequently, diluted BG4 antibody (1:10; Sigma, Shanghai, China) was used to incubate with extracted nuclei in ice for 6 h. The BG4 was probed by anti-FLAG epitope tag antibody (1:50; Sigma, Shanghai, China) at 4 °C overnight. Anti-rabbit IgG secondary antibody (Vazyme, Nanjing, China) was used to bind BG4 at room temperature for 1 h. pA/G-Tnp was used to bind with IgG for 1 h, and the genome was excised by transposase at 37 °C for 1 h. Finally, the genomic DNA fragments were extracted and purified with DNA Extract Beads and stored at − 80 °C.

The purified DNA fragments were used in library amplification using TruePrep Index Kit V2 for Illumina (Vazyme, Nanjing, China) according to the associated protocol. The amplified products were purified using VAHTS DNA Clean Beads (Vazyme, Nanjing, China) according to the instruction to obtain sequencing library. Agilent Technologies 2100 Bioanalyzer (Agilent, CA, US) was used for library quality control. Sequencing was performed on the Illumina platform. Bioinformatic analysis was conducted using the OECloud tools at (https://cloud.oebiotech.com). The genome for mapping was GRCg7b (accessed link: http://ftp.ncbi.nlm.nih.gov/genomes/). The raw data obtained from this sequencing was submitted in SRA database (submission ID: PRJNA1022420).

Whole genome bisulfite sequencing (WGBS) library construction

For WGBS library construction, the same batch samples were collected for DNA extraction. After DNA quality detection, the genomic DNA was randomly fragmented in the range of 200 bp to 300 bp. The ends of the interrupted DNA were repaired; A-tail and sequencing adaptor with all cytosine methylated were added. The DNA were then treated with bisulfite using the EZ DNA Methylation-Glod Kits (Zymo Research, Irvine, CA, USA). After PCR amplification and product purification, the library sequencing was performed on the Illumina NovaSeq 6000 platform (Illumina Inc., San Diego,

CA, USA). Sequencing and analysis were performed by OE Biotech Co., Ltd. (Shanghai, China). The raw data were submitted to the SRA database (accessed ID: PRJNA1025099).

Bioinformatic analysis was performed using the OECloud tools at (https://cloud.oebiotech.com). Clean reads were aligned to the reference genome (GRCg7b) using Bismark. Differentially methylated regions (DMRs) were analyzed using MethylKit, with region window size = 1000 bp and step size = 1000 bp. $P < 0.05$ and difference ≥ 10% were set as the cutoff for significant DMRs. The promoter region was defined as 2000 bp upstream of the TSS of a gene and the differentially methylated promoters were analyzed with the same criterion for DMRs.

RNA-seq

Total RNA was extracted from the same batch samples using TRIzol reagent (Takara, Toyoko, Japan). Following RNA quality detection, the library was constructed using VAHTS Universal V6 RNA-seq Library Prep Kit according to the instruction. Illumina Novaseq 6000 platform was used for sequencing. The data obtained from this sequencing was submitted to SRA database (accessed ID: PRJNA1023305). The clean reads were mapped to chicken genome (GRCg7b). Differential expression genes (DEGs) analysis was carried out and P-value < 0.05 and |log2FC| > 1 were considered as the cutoff for DEGs. Transcriptome sequencing and analysis were conducted by OE Biotech Co., Ltd. (Shanghai, China).

Immunofluorescence staining

MyHC immunofluorescence staining was used to quantify myoblast differentiation. After treatment with PDS with different concentrations, myoblasts were cultured in differentiation medium for 3 days. The cells were fixed in 4% paraformaldehyde (Solarbio, Beijing, China) for 30 min at room temperature, permeabilized with 0.1% Triton-X100 (Solarbio, Beijing, China) for 10 min at room temperature, and then blocked in 5% goat serum (Solarbio, Beijing, China) for 1 h at room temperature. Then the MyHC antibody (1:50; DSHB) was incubated overnight at 4 °C. On the following day, anti-mouse FITC-conjugated (1:200; CST, MA, USA) secondary antibody was incubated for 1 h at room temperature. Nuclei were counterstained with 4,6-diamidino-2-phenylindole dihydrochloride (DAPI, Solarbio, Beijing, China). Finally, the cells were captured in a Leica fluorescence microscope.

G4 immunofluorescence staining was used to examine the difference in myoblasts before and after differentiation. Following treatment of myoblasts with growth medium, myoblasts were treated with differentiation medium for 3 days and they were fixed in 2% paraformaldehyde (Solarbio, Beijing, China) for 30 min at 4 °C. Myoblasts were permeabilized with 0.1% Triton-X100 (Solarbio, Beijing, China) for 30 min at 4 °C and then blocked in 5% BSA (Solarbio, Beijing, China) overnight at 4 °C. BG4 antibody (1:50; Sigma, Shanghai, China) was then incubated overnight at 4 °C. Anti-rabbit Alexa 594-conjugated (1:1000; CST, MA, USA) secondary antibody was incubated for 1 h at room temperature. After washing four times with 0.1% Tween-20, the coverslips were mounted with Gold/DAPI (Solarbio, Beijing, China), and confocal images were acquired and viewed with a Leica DMi8 confocal microscope. Cells were washed for G4 positive cell quantification in a flow cytometry (Beckman, Brea, CA, USA) and the data were analyzed using FlowJo software.

Polymerase stop assay (PSA)

PSA was performed using *NFATC2* G4 sequence or its mutant sequence as a template. The template DNA was synthesized by TSINGKE. The DNA was diluted in 50 nM Tris–HCl (pH7.4) with 100 mM KCl and heated at 95 °C for 15 min, then cooled to room temperature over 4 h to allow G4 structure to form. Varying amounts of PDS were used to incubate with an annealed template at room temperature. PCR was performed using 2 × AceTaq Master Mix (Dye Plus) (Vazyme, Nanjing, China) and the product was separated in a 4–20% denaturing polyacrylamide gel (TSINGKE, Guangzhou, China). The concentration of template and primer were 10 μM and 2.5 μM, respectively. The single-stranded DNA of the G4 sequence and its mutant sequence were synthesized by TSINGKE. The primer was labelled with FAM at 5' terminal. The oligonucleotides used in this study are listed in Additional file 2: Table S8.

Statistical analysis

Statistical analysis was executed in Prism GraphPad 9.5. The data presented in this study was shown as mean ± SEM and differences between groups were analyzed using a two-tailed t-test. The level of significance was presented as *($P < 0.05$), **($P < 0.01$), ***($P < 0.001$), and **** ($P < 0.0001$).

Abbreviations

ASO	Antisense oligonucleotide
CCNB2	Cyclin B2
CCND1	Cyclin D1
CDKN1B	Cyclin-dependent kinase inhibitor 1B
Cut&Tag	Cleavage under targets and tagmentation
DEG	Differentially expressed gene
DM	Differentiation medium
DMR	Differentially methylated region
DP	Differential peak
EdU	5-Ethynyl-2′-deoxyuridine
G4	G-quadruplex
GM	Growth medium
HRH3	Histamine receptor H3
IDI2	Isopentenyl-diphosphate delta isomerase 2

MBP	Myelin basic protein
MSP	Methylation-specific PCR
MYOCD	Myocardin
MyoD1	Myogenic differentiation 1
MyoG	Myogenin
MYH1G	Myosin heavy chain 1G
MyHC	Myosin heavy chain
NFATC2	Nuclear factor of activated T cells 2
PDS	Pyridostatin
PLA2G4A	Phospholipase A2 group IVA
PQS	Potential quadruplex sequence
PSA	Polymerase stop assay
RPESP	Somatomedin B and thrombospondin type 1 domain containing
TGFBR2	Transforming growth factor beta receptor 2
TMOD1	Tropomodulin 1
WGBS	Whole-genome bisulfite sequencing

Supplementary Information

The online version contains supplementary material available at https://doi.org/10.1186/s12915-024-01993-z.

Additional file 1: Figure S1-S5. Fig.S1 - G4 density during myoblast differentiation and PDS effect on Desmin. Fig.S2 - G4 Cut & Tag products size and distribution. Fig.S3 - G4 PQSs schematic diagram in MyoD1 promoter. Fig. S4 - CpG-, CHH- and CHG-type methyl modification distribution information. Fig.S5 - The GO and KEGG enrichment analysis for DMRs. Fig.S6 - PQSs prediction for *PLA2G4A*.

Additional file 2: Table S1-S8. Table S1 - Cut & Tag sequencing data overview. Table S2 - DPs between GM and DM. Table S3 - RNA-seq data overview. Table S4 - The DEGs between GM and DM. Table S5 - The GO terms DEGs enriched in. Table S6 - Integrating analysis for DPs and DEGs. Table S7 - WGBS data overview. Table S8 - The information of oligonucleotides used in this study.

Additional file 3: Original images for western blot.

Acknowledgements
Not applicable.

Authors' contributions
LG was responsible for research designing, cellular experiments, data analysis, and manuscript draft. WH participated in part of flow cytometry analysis and bioinformatic analysis. QW and SZ performed part of cellular experiments. FB participated in data analysis and manuscript drafting. ZX participated in the manuscript revision and part of the experiments. QN designed the experiments, analyzed data, and participated in the manuscript revision. All authors read and approved the final manuscript.

Funding
This study was supported by the National Key R&D Program of China (2021YFD1300100), Local Innovative and Research Teams Project of Guangdong Province (2019BT02N630), China Agriculture Research System (CARS-41-G03), STI2030-Major Projects (2023ZD0406405), and China Postdoctoral Science Foundation (2023M731145).

Availability of data and materials
The datasets generated during the current study are available in the SRA database (https://www.ncbi.nlm.nih.gov/sra/) with the accession ID PRJNA1025099 [61], PRJNA1022420 [62], and PRJNA1023305 [63]. Other data are available from the corresponding author on reasonable request.

Declarations

Ethics approval and consent to participate
All Institutional and National Guidelines for the care and use of animals were followed in this study. All animal experiments in this research were approved by the Animal Welfare Committee of South China Agricultural University (Approved ID: SCAU#2021F074).

Consent for publication
Not applicable.

Competing interests
The authors declare that they have no competing interests.

Received: 6 March 2024 Accepted: 27 August 2024
Published online: 11 September 2024

References

1. Dingley AJ, Peterson RD, Grzesiek S, Feigon J. Characterization of the cation and temperature dependence of DNA quadruplex hydrogen bond properties using high-resolution NMR. J Am Chem Soc. 2005;127:14466–72.
2. Schaffitzel C, Berger I, Postberg J, Hanes J, Lipps HJ, Plückthun A. In vitro generated antibodies specific for telomeric guanine-quadruplex DNA react with Stylonychia lemnae macronuclei. Proc Natl Acad Sci U S A. 2001;98:8572–7.
3. Siddiqui-Jain A, Grand CL, Bearss DJ, Hurley LH. Direct evidence for a G-quadruplex in a promoter region and its targeting with a small molecule to repress c-MYC transcription. Proc Natl Acad Sci U S A. 2002;99:11593–8.
4. Besnard E, Babled A, Lapasset L, Milhavet O, Parrinello H, Dantec C, et al. Unraveling cell type-specific and reprogrammable human replication origin signatures associated with G-quadruplex consensus motifs. Nat Struct Mol Biol. 2012;19:837–44.
5. Lin W, Sampathi S, Dai H, Liu C, Zhou M, Hu J, et al. Mammalian DNA2 helicase/nuclease cleaves G-quadruplex DNA and is required for telomere integrity. EMBO J. 2013;32:1425–39.
6. Choi J, Majima T. Conformational changes of non-B DNA. Chem Soc Rev. 2011;40:5893–909.
7. Bugaut A, Balasubramanian S. 5'-UTR RNA G-quadruplexes: translation regulation and targeting. Nucleic Acids Res. 2012;40:4727–41.
8. Rawal P, Kummarasetti VBR, Ravindran J, Kumar N, Halder K, Sharma R, et al. Genome-wide prediction of G4 DNA as regulatory motifs: role in Escherichia coli global regulation. Genome Res. 2006;16:644–55.
9. Rankin S, Reszka AP, Huppert J, Zloh M, Parkinson GN, Todd AK, et al. Putative DNA quadruplex formation within the human c-kit oncogene. J Am Chem Soc. 2005;127:10584–9.
10. Hänsel-Hertsch R, Di Antonio M, Balasubramanian S. DNA G-quadruplexes in the human genome: detection, functions and therapeutic potential. Nat Rev Mol Cell Biol. 2017;18:279–84.
11. Müller S, Sanders DA, Di Antonio M, Matsis S, Riou JF, Rodriguez R, et al. Pyridostatin analogues promote telomere dysfunction and long-term growth inhibition in human cancer cells. Org Biomol Chem. 2012;10:6537–46.
12. Rodriguez R, Miller KM, Forment JV, Bradshaw CR, Nikan M, Britton S, et al. Small-molecule-induced DNA damage identifies alternative DNA structures in human genes. Nat Chem Biol. 2012;8:301–10.
13. Grand CL, Han H, Muñoz RM, Weitman S, Von Hoff DD, Hurley LH, et al. The cationic porphyrin TMPyP4 down-regulates c-MYC and human telomerase reverse transcriptase expression and inhibits tumor growth in vivo. Mol Cancer Ther. 2002;1:565–73.
14. Guilbaud G, Murat P, Recolin B, Campbell BC, Maiter A, Sale JE, et al. Local epigenetic reprogramming induced by G-quadruplex ligands. Nat Chem. 2017;9:1110–7.
15. Drygin D, Siddiqui-Jain A, O'Brien S, Schwaebe M, Lin A, Bliesath J, et al. Anticancer activity of CX-3543: a direct inhibitor of rRNA biogenesis. Cancer Res. 2009;69:7653–61.
16. Xu H, Di Antonio M, McKinney S, Mathew V, Ho B, O'Neil NJ, et al. CX-5461 is a DNA G-quadruplex stabilizer with selective lethality in BRCA1/2 deficient tumours. Nat Commun. 2017;8:14432.
17. Marsico G, Chambers VS, Sahakyan AB, McCauley P, Boutell JM, Antonio MD, et al. Whole genome experimental maps of DNA G-quadruplexes in multiple species. Nucleic Acids Res. 2019;47:3862–74.
18. Niu K, Zhang X, Deng H, Wu F, Ren Y, Xiang H, et al. BmILF and i-motif structure are involved in transcriptional regulation of BmPOUM2 in Bombyx mori. Nucleic Acids Res. 2018;46:1710–23.

19. Cheng Y, Tang Q, Li Y, Zhang Y, Zhao C, Yan J, et al. Folding/unfolding kinetics of G-quadruplexes upstream of the P1 promoter of the human BCL-2 oncogene. J Biol Chem. 2019;294:5890–5.
20. Zhang X, Zhao B, Yan T, Hao A, Gao Y, Li D, et al. G-quadruplex structures at the promoter of HOXC10 regulate its expression. Biochim Biophys Acta Gene Regul Mech. 2018;1861:1018–28.
21. Scaal M, Marcelle C. Chick muscle development. Int J Dev Biol. 2018;62:127–36.
22. Zammit PS. Function of the myogenic regulatory factors Myf5, MyoD, Myogenin and MRF4 in skeletal muscle, satellite cells and regenerative myogenesis. Semin Cell Dev Biol. 2017;72:19–32.
23. Weintraub H, Davis R, Tapscott S, Thayer M, Krause M, Benezra R, et al. The myoD gene family: nodal point during specification of the muscle cell lineage. Science. 1991;251:761–6.
24. Comai G, Tajbakhsh S. Molecular and cellular regulation of skeletal myogenesis. In: Current Topics in Developmental Biology. Elsevier; 2014. page 1–73. Available from: https://linkinghub.elsevier.com/retrieve/pii/B9780124059436000014. Cited 2023 Sep 13.
25. Lehka L, Rędowicz MJ. Mechanisms regulating myoblast fusion: a multilevel interplay. Semin Cell Dev Biol. 2020;104:81–92.
26. Zyner KG, Simeone A, Flynn SM, Doyle C, Marsico G, Adhikari S, et al. G-quadruplex DNA structures in human stem cells and differentiation. Nat Commun. 2022;13:142.
27. Testa S, D'Addabbo P, Fornetti E, Belli R, Fuoco C, Bernardini S, et al. Myoblast myogenic differentiation but not fusion process is inhibited via MyoD tetraplex interaction. Oxid Med Cell Longev. 2018;2018: e7640272.
28. Ciszewski L, Lu-Nguyen N, Slater A, Brennan A, Williams HEL, Dickson G, et al. G-quadruplex ligands mediate downregulation of DUX4 expression. Nucleic Acids Res. 2020;48:4179–94.
29. Chen X, Yuan J, Xue G, Campanario S, Wang D, Wang W, et al. Translational control by DHX36 binding to 5′UTR G-quadruplex is essential for muscle stem-cell regenerative functions. Nat Commun. 2021;12:5043.
30. Umar MI, Chan CY, Kwok CK. Development of RNA G-quadruplex (rG4)-targeting L-RNA aptamers by rG4-SELEX. Nat Protoc. 2022;17:1385–414.
31. Lavezzo E, Berselli M, Frasson I, Perrone R, Palù G, Brazzale AR, et al. G-quadruplex forming sequences in the genome of all known human viruses: a comprehensive guide. PLoS Comput Biol. 2018;14: e1006675.
32. Capra JA, Paeschke K, Singh M, Zakian VA. G-quadruplex DNA sequences are evolutionarily conserved and associated with distinct genomic features in Saccharomyces cerevisiae. PLoS Comput Biol. 2010;6: e1000861.
33. Wu F, Niu K, Cui Y, Li C, Lyu M, Ren Y, et al. Genome-wide analysis of DNA G-quadruplex motifs across 37 species provides insights into G4 evolution. Commun Biol. 2021;4:98.
34. Zhao Y, Du Z, Li N. Extensive selection for the enrichment of G4 DNA motifs in transcriptional regulatory regions of warm blooded animals. FEBS Lett. 2007;581:1951–6.
35. Illingworth R, Kerr A, Desousa D, Jørgensen H, Ellis P, Stalker J, et al. A novel CpG island set identifies tissue-specific methylation at developmental gene loci. PLoS Biol. 2008;6: e22.
36. Tsukakoshi K, Saito S, Yoshida W, Goto S, Ikebukuro K. CpG Methylation changes G-quadruplex structures derived from gene promoters and interaction with VEGF and SP1. Molecules. 2018;23:944.
37. Huang RX, Zhou PK. DNA damage response signaling pathways and targets for radiotherapy sensitization in cancer. Signal Transduct Target Ther. 2020;5:60.
38. Kaya-Okur HS, Wu SJ, Codomo CA, Pledger ES, Bryson TD, Henikoff JG, et al. CUT&Tag for efficient epigenomic profiling of small samples and single cells. Nat Commun. 2019;10:1930.
39. Li C, Wang H, Yin Z, Fang P, Xiao R, Xiang Y, et al. Ligand-induced native G-quadruplex stabilization impairs transcription initiation. Genome Res. 2021;31:1546–60.
40. Stark R, Grzelak M, Hadfield J. RNA sequencing: the teenage years. Nat Rev Genet. 2019;20:631–56.
41. Li Y, Tollefsbol TO. DNA methylation detection: bisulfite genomic sequencing analysis. Methods Mol Biol. 2011;791:11–21.
42. Chargé S, Rudnicki MA. Fusion with the fused: a new role for interleukin-4 in the building of muscle. Cell. 2003;113:422–3.
43. Peng Y, Du J, Günther S, Guo X, Wang S, Schneider A, et al. Mechano-signaling via Piezo1 prevents activation and p53-mediated senescence of muscle stem cells. Redox Biol. 2022;52: 102309.
44. Karppinen S, Rapila R, Naumenko N, Tuomainen T, Koivumäki JT, Hänninen SL, et al. Ca(2+)-activated K(+) current is essential for maintaining excitability and gene transcription in early embryonic cardiomyocytes. Acta Physiol (Oxf). 2016;216:101–11.
45. Dryer SE, Lhuillier L, Cameron JS, Martin-Caraballo M. Expression of K(Ca) channels in identified populations of developing vertebrate neurons: role of neurotrophic factors and activity. J Physiol Paris. 2003;97:49–58.
46. Fay MM, Lyons SM, Ivanov P. RNA G-quadruplexes in Biology: principles and molecular mechanisms. J Mol Biol. 2017;429:2127–47.
47. Lejault P, Moruno-Manchon JF, Vemu SM, Honarpisheh P, Zhu L, Kim N, et al. Regulation of autophagy by DNA G-quadruplexes. Autophagy. 2020;16:2252–9.
48. Du Z, Kong P, Gao Y, Li N. Enrichment of G4 DNA motif in transcriptional regulatory region of chicken genome. Biochem Biophys Res Commun. 2007;354:1067–70.
49. Wang C, Yue F, Kuang S. Muscle histology characterization using H&E staining and muscle fiber type classification using immunofluorescence staining. Bio Protoc. 2017;7: e2279.
50. Ochala J, Finno CJ, Valberg SJ. Myofibre Hyper-Contractility in Horses Expressing the Myosin Heavy Chain Myopathy Mutation, MYH1E321G. Cells. 2021;10:3428.
51. McElhinny AS, Kolmerer B, Fowler VM, Labeit S, Gregorio CC. The N-terminal end of nebulin interacts with tropomodulin at the pointed ends of the thin filaments. J Biol Chem. 2001;276:583–92.
52. Gokhin DS, Lewis RA, McKeown CR, Nowak RB, Kim NE, Littlefield RS, et al. Tropomodulin isoforms regulate thin filament pointed-end capping and skeletal muscle physiology. J Cell Biol. 2010;189:95–109.
53. Ono Y, Schwach C, Antin PB, Gregorio CC. Disruption in the tropomodulin1 (Tmod1) gene compromises cardiomyocyte development in murine embryonic stem cells by arresting myofibril maturation. Dev Biol. 2005;282:336–48.
54. Mao SQ, Ghanbarian AT, Spiegel J, Martínez Cuesta S, Beraldi D, Di Antonio M, et al. DNA G-quadruplex structures mold the DNA methylome. Nat Struct Mol Biol. 2018;25:951–7.
55. Matsumoto S, Tateishi-Karimata H, Sugimoto N. DNA methylation is regulated by both the stability and topology of G-quadruplex. Chem Commun (Camb). 2022;58:12459–62.
56. Lyu J, Shao R, Kwong Yung PY, Elsässer SJ. Genome-wide mapping of G-quadruplex structures with CUT&Tag. Nucleic Acids Res. 2022;50: e13.
57. Daou N, Lecolle S, Lefebvre S, della Gaspera B, Charbonnier F, Chanoine C, et al. A new role for the calcineurin/NFAT pathway in neonatal myosin heavy chain expression via the NFATc2/MyoD complex during mouse myogenesis. Development 2013;140:4914–25.
58. Der Vartanian A, Chabanais J, Carrion C, Maftah A, Germot A. Downregulation of POFUT1 impairs secondary myogenic fusion through a reduced NFATc2/IL-4 signaling pathway. Int J Mol Sci. 2019;20:4396.
59. Kurosaka M, Hung YL, Machida S, Kohda K. IL-4 signaling promotes myoblast differentiation and fusion by enhancing the expression of MyoD, Myogenin, and Myomerger. Cells. 2023;12:1284.
60. Guo L, Huang W, Chen B, Jebessa Bekele E, Chen X, Cai B, et al. gga-mir-133a-3p regulates myoblasts proliferation and differentiation by targeting PRRX1. Front Genet. 2018;9:577.
61. Guo L. WGBS for chicken myoblast DM_vs_GM. Bioproject accession: PRJNA1025099 (2023). https://www.ncbi.nlm.nih.gov/bioproject/?term=prjna1025099.
62. Guo L. Global G4s genomic landscape during embryonic myogenesis in chicken. Bioproject accession: PRJNA1022420 (2023). https://www.ncbi.nlm.nih.gov/bioproject/?term=PRJNA1022420.
63. Guo L. RNA-seq for chicken myoblast GM_vs_DM. Bioproject accession: PRJNA1023305 (2023). https://www.ncbi.nlm.nih.gov/bioproject/?term=PRJNA1023305.

Publisher's Note